PHYSICAL REVIEW D **81,** 044040 (2010)

Well-posedness, linear perturbations, and mass conservation for the axisymmetric Einstein equations

Sergio Dain

Facultad de Matemática, Astronomía y Física, FaMAF, Universidad Nacional de Córdoba, Instituto de Física Enrique Gaviola, IFEG, CONICET, Ciudad Universitaria (5000) Córdoba, Argentina, and Max Planck Institute for Gravitational Physics (Albert-Einstein-Institut) Am Mühlenberg 1 D-14476 Potsdam Germany

Omar E. Ortiz

Facultad de Matemática, Astronomía y Física, FaMAF, Universidad Nacional de Córdoba, Instituto de Física Enrique Gaviola, IFEG, CONICET, Ciudad Universitaria (5000) Córdoba, Argentina

(Received 18 December 2009; published 26 February 2010)

For axially symmetric solutions of Einstein equations there exists a gauge which has the remarkable property that the total mass can be written as a conserved, positive definite, integral on the spacelike slices. The mass integral provides a nonlinear control of the variables along the whole evolution. In this gauge, Einstein equations reduce to a coupled hyperbolic-elliptic system which is formally singular at the axis. As a first step in analyzing this system of equations we study linear perturbations on a flat background. We prove that the linear equations reduce to a very simple system of equations which provide, though the mass formula, useful insight into the structure of the full system. However, the singular behavior of the coefficients at the axis makes the study of this linear system difficult from the analytical point of view. In order to understand the behavior of the solutions, we study the numerical evolution of them. We provide strong numerical evidence that the system is well-posed and that its solutions have the expected behavior. Finally, this linear system allows us to formulate a model problem which is physically interesting in itself, since it is connected with the linear stability of black hole solutions in axial symmetry. This model can contribute significantly to solve the nonlinear problem and at the same time it appears to be tractable.

DOI: 10.1103/PhysRevD.81.044040 PACS numbers: 04.20.Ex, 04.25.D−, 02.30.Jr

I. INTRODUCTION

Axisymmetric spacetimes have been studied mainly for two reasons. The first one is that they often appear in astrophysical models like rotating stars and black holes. The second is because in the presence of any symmetry Einstein equations simplify considerably and hence these spacetimes are useful as an intermediate step to understand more complex problems. In particular, axially symmetric gravitational waves in vacuum do not carry angular momentum; this represents an important simplification in the dynamics. Also, axial symmetry is the only symmetry compatible with asymptotic flatness and nontrivial gravitational radiation [1]. From this perspective, axially symmetric gravitational waves are the simplest possible waves emitted from isolated sources. And hence these waves represent the natural candidates to study the strong field dynamics of gravitational waves in Einstein equations.

However, axial symmetry presents a major difficulty. To take advantage of the symmetry an adapted coordinate system should be used in order to reduce the field equations to a lower-dimensional system (there is a well-known procedure to do this for any symmetry in a geometrical way [2]; we review this result in Sec. III A). The difficulty arises because the norm of the axial Killing vector vanishes at the axis, and hence the reduced equations are formally singular there.

This difficulty is so severe that until recently axially symmetric spacetimes have not been studied in detail even using numerical techniques (see chapter 10.4 in [3] and references therein). In a number of recent articles [4–8] these kinds of singular systems have been successfully solved numerically. There is however no analytical study of axial symmetry in the dynamical regime (see the review article [9] for results for other kind of symmetries). In fact, it can be argued that this singular behavior near the axis is so complicated that the axially symmetric case is as hard as the full general case from the analytical point of view.

There exists however a new ingredient that makes, in our opinion, the problem worth studying. In the article [10] it has been proved that there exists a gauge in axial symmetry such that the total mass of the spacetime can be written as a positive definite volume integral over the spacelike slices of the foliation. Moreover, this integral is conserved along the evolution. This conserved integral controls the norm of the fields along the whole evolution. This is certainly a very desirable property of this gauge which is not present in the general, nonsymmetric, case. Also, this mass integral formula appears to be connected with stability properties of black holes in axial symmetry [11].

The gauge mentioned above is a combination of the well-known maximal condition for the lapse and the choice of isothermal coordinates (also called quasi isotropical) for the shift. The later condition is only possible in axial

symmetry. We call this gauge the maximal-isothermal gauge. This gauge has been known for long time (see [12,13]) but without noticing this property of the mass. It is also important to emphasize that this gauge is the one used in most of the recent numerical computations [4–7] (examples of other gauge choices in axial symmetry are given in [14,15]). That is, this gauge has not only desirable analytical properties but it is also useful for numerical studies.

The very basic question of well-posedness of the equations in this gauge is open. This question is rather subtle because of the singular behavior mentioned above. The standard theory in partial differential equations does not seem to apply in a direct way. This is the problem we want to study in this article. In order to do this, the first step is to study the linearization of the equations around fixed solutions. We choose Minkowski as a background for simplicity. As we describe in the next section, we obtain a remarkable simple system of linear equations together with a conserved quantity which corresponds to the mass of the spacetime up to second-order corrections. This system allows us to formulate the problem of well-posedness in a simplified setting which is nevertheless relevant and physically interesting. Remarkably enough, even for this linear system the well-posedness appears to be a nontrivial problem. In order to get insight into this problem we numerically evolve these equations to provide evidence that the system is in fact well-posed and that the solutions have the expected behavior.

Being that the local existence problem is so complicated in this gauge one can wonder what can be said about the global behavior of the evolution, which is, of course, the ultimate goal. However, many of the main complications of this gauge are already present in the well-posedness problem because they are related to the local behavior of the fields at the symmetry axis. If one can sort out the difficulties for the linearized system in a satisfactory way there is a good chance that the mass integral formula can be used to control the global evolution in some way. Also, the well-posedness of the linear equations is relevant in itself for the following two reasons. First, the mass formula at the linear level can in principle be used to prove linear stability in axial symmetry of a background solution like a black hole. Second, the well-posedness of the linear equations and the mass formula give insight on appropriate boundary conditions on a bounded domain. In particular, the mass formula allows us to calculate the gravitational waves that leave or enter a bounded domain.

The plan of the article is the following. In Sec. II we summarize our main results. In Sec. III we review the axially symmetric, vacuum, Einstein equations. Although this is well known, the way we proceed to obtain the final equations in the maximal-isothermal gauge is slightly different than the standard one used in the numerical works mentioned above. In Sec. IV we derive our main linear equations, and in Sec. V we describe their main properties. In particular, in this section we discuss the mass conservation and boundary conditions on a bounded domain. In Sec. VI we describe the numerical techniques used to evolve these equations. And in Sec. VII we present the numerical results. Finally, in Sec. VIII we conclude with a discussion of the relevant open problems.

II. MAIN RESULTS

This article has two main results. The first one is to prove that the linearized Einstein vacuum equations in the maximal-isothermal gauge reduce to a very simple set of equations together with a conserved quantity. This conserved quantity is the mass up to second-order corrections and it is written as a positive definite integral over a spacelike surface, which has a similar form to the energy of the wave equation. This property of the mass, which only holds in this gauge, is of course what distinguished this system of equations from any other linearization.

The second result is the numerical study of these equations, together with the analysis of appropriate boundary conditions on a finite grid.

Let us describe the first result. In axial symmetry, the dynamical degrees of freedom of the vacuum gravitational field are prescribed by two functions, which can be chosen to be the norm and twist potential of the axial Killing vector (see Sec. III). We make, for simplicity, the extra assumption that the twist is zero (although we discuss the full nonlinear equations with twist in Sec. III). This assumption simplifies the equations, but it is by no means essential. In the maximal-isothermal gauge, the linearized Einstein equations with respect to a Minkowski background reduce to the following two equations for the functions v and β^ρ (the reason for the notation for the last function is that it represents the ρ component of the shift vector as we will see below):

$$\ddot{v} = \Delta v - \frac{\partial_\rho v}{\rho} + \rho \partial_\rho \left(\frac{\beta^\rho}{\rho} \right), \tag{1}$$

$$\Delta \beta^\rho = \frac{2}{\rho} \left(\Delta v - \frac{\partial_\rho v}{\rho} \right). \tag{2}$$

These equations are deduced in Sec. IV. We have chosen cylindrical coordinates (t, ρ, z). The relevant domain for these equations is the half plane $\rho \geq 0$, $-\infty < z < \infty$, denoted by $\mathbb{R}^2_+$. A dot denotes the time derivative and Δ is the flat Laplacian in two dimensions:

$$\Delta v = \partial^2_\rho v + \partial^2_z v. \tag{3}$$

The boundary conditions for Eqs. (1) and (2) arise from the regularity of the spacetime metric at the axis and the standard asymptotically flat falloff behavior at infinity. We discuss this in detail in Sec. III D and V. Let us present here a summary. Equation (2) is an elliptic equation for β^ρ; we need to prescribe boundary conditions on $\mathbb{R}^2_+$. On the

axis $\rho = 0$ we require

$$\beta^\rho|_{\rho=0} = 0, \tag{4}$$

and at infinity we impose

$$\beta^\rho = O(r^{-1}), \tag{5}$$

where $r = \sqrt{\rho^2 + z^2}$. With these boundary conditions, Eq. (2) has a unique solution. Equation (1) is a wave equation for υ; we need to prescribe initial conditions, which are functions $f(\rho, z)$ and $g(\rho, z)$ such that

$$\upsilon|_{t=0} = f, \qquad \dot{\upsilon}|_{t=0} = g. \tag{6}$$

The axis represents a timelike boundary for the wave Eq. (1), and hence we need to prescribe also boundary conditions there. This is the delicate part, because the equations are singular at the axis and hence we are not free to chose arbitrary boundary conditions there. From the axial regularity of the spacetime metric we deduce that the initial data f and g should vanish at the axis, namely

$$f|_{\rho=0} = 0, \qquad g|_{\rho=0} = 0. \tag{7}$$

In Sec. V, using series expansions, we prove that conditions (7) on the initial data imply that

$$\upsilon|_{\rho=0} = 0, \qquad \partial_\rho \upsilon|_{\rho=0} = 0, \tag{8}$$

for all times. Moreover, solutions υ and β^ρ of Eqs. (1) and (2) satisfy parity conditions; namely υ is an even function of ρ and β^ρ is an odd function of ρ. These parity conditions imply that the spacetime metric is smooth at the axis. It is important to emphasize that these conditions are consequences of Eqs. (1) and (2) alone, without any extra requirement.

In the numerical implementation, Eqs. (8) are used as boundary conditions at the axis. There are various ways to reexpress (1) and (2) in order write conditions (8) as proper timelike boundary conditions (e.g. Dirichlet or Neumann). For example, following [4], in Sec. VI we write them in terms of the rescaled variable $\bar{\upsilon} = \upsilon/\rho$.

We are interested in asymptotically flat solutions of (1) and (2). We will argue in Sec. V, that the typical falloff behavior as $r \to \infty$ for this kind of solutions is

$$\upsilon = O(r^{-2}). \tag{9}$$

That is, if we chose initial data f and g which satisfy (9) then υ will satisfy (9) for all times.

All the other components of the linear perturbation can be calculated in terms of υ and β^ρ as follows. In our gauge the four-dimensional coordinates are given by (t, ρ, z, ϕ). A general twist-free linear perturbation is written as follows:

$$\gamma = (\sigma + 2q)(d\rho^2 + dz^2) + 2\beta^\rho d\rho dt + 2\beta^z dz dt + \rho^2 \sigma d\phi^2, \tag{10}$$

where the functions σ, q, β^ρ and β^z depend only on (t, ρ, z). The function β^ρ is given by (2); the other functions are calculated in terms of υ as follows. The function q is a time derivative of υ:

$$q = \dot{\upsilon}. \tag{11}$$

The function σ is determined by the following elliptic equation:

$${}^{(3)}\Delta\sigma = -\Delta\dot{\upsilon}, \tag{12}$$

where ${}^{(3)}\Delta$ is defined as

$${}^{(3)}\Delta\sigma = \Delta\sigma + \frac{\partial_\rho \sigma}{\rho}. \tag{13}$$

This operator, which appears frequently in the rest of the article, is the flat Laplace operator in three dimensions written in cylindrical coordinates and acting on axially symmetric functions. The boundary condition for Eq. (12) at the axis is given by

$$\partial_\rho \sigma|_{\rho=0} = 0, \tag{14}$$

and at infinity we impose

$$\sigma = O(r^{-1}). \tag{15}$$

Equation (12) can be also viewed as an equation in $\mathbb{R}^3$. In this case we do not need to prescribe any boundary condition at the axis. Condition (14) will be automatically satisfied for any regular solution.

Finally, the other component of the shift vector is determined by the following equation:

$$\Delta\beta^z = -2\frac{\partial_z \upsilon}{\rho^2}, \tag{16}$$

with boundary condition at the axis

$$\partial_\rho \beta^z|_{\rho=0} = 0, \tag{17}$$

and decay condition at infinity

$$\beta^z = O(r^{-1}). \tag{18}$$

The total mass of the system is given by the following integral:

$$m = \frac{1}{16}\int_{\mathbb{R}^2_+} \left(4\frac{|\partial\upsilon|^2}{\rho^2} + (\Delta\upsilon)^2 + |\partial\sigma|^2\right)\rho d\rho dz. \tag{19}$$

Note that in order to compute the mass we need the function σ, which satisfies Eq. (12). This equation is uncoupled with Eqs. (1) and (2). The integral (19) is conserved. That is, for every solution of (1) and (2) which satisfies the boundary conditions (4), (5), and (8) and decay like (9) at infinity we have

$$\dot{m} = 0. \tag{20}$$

The conservation law (20) is deduced from a local conservation formula which involves the integrand of the mass formula (19). This local conservation law can be also used

to compute the gravitational waves entering or leaving a bounded domain. We discuss this in Sec. V.

The second main result of this article is the numerical study of the system (1) and (2). We describe this in detail in Sec. VII. Let us briefly summarize these results. The system (1) and (2) appears, from the numerical evidences, to be well-posed and out implementation numerically stable. In particular, this implies that the functions υ and β^ρ remain bounded for all times by a constant that depends only on the initial data. This is consistent with the linear stability of Minkowski spacetime.

The numerical calculations are, of course, performed on a finite grid. Hence, we need to prescribe boundary conditions on a bounded domain. These conditions should be compatible with asymptotical flatness in the following sense. Assume we have a sequence of bounded domains such that in the limit they cover the half plane $\mathbb{R}^2_+$. If we solved the equations for this sequence of domains we should recover in the limit the asymptotically flat solution described above. There exists many different boundary conditions that have this property: in particular, homogeneous Dirichlet conditions for β^ρ and υ. For each bounded domain the mass is not conserved. However, as the size of the domain increases we expect that the mass approaches a time-independent constant. This is precisely what we observe in our numerical calculations.

For our present goal, this kind of asymptotically flat boundary condition is all that we need. There is, however, an interesting extra point here. To model an isolated system on a finite grid it is important to prescribe boundary conditions such that the gravitational radiation leaves the domain. In general, this is a very difficult problem since it is not even clear what we mean by gravitational radiation at a finite distance. However, as we mention above, in our gauge the mass formula allows us to compute gravitational radiation on a bounded domain. Although it appears not to be possible to prescribe boundary conditions such that the gravitational waves always leave the domain, the mass formula suggests a particular kind of boundary condition that has this behavior in our numerical calculations. That is, under these boundary conditions, the mass on a bounded domain is monotonically decreasing with time for the particular kind of initial data used in the computations. We emphasize however that we have not been able to prove this analytically. We explore this in detail in Secs. V and VII.

III. AXISYMMETRIC VACUUM EINSTEIN EQUATIONS

The purpose of this section is to write the vacuum Einstein equations for axially symmetric spacetimes in the maximal-isothermal gauge. This involves three clearly distinguished steps. In the first one, described in Sec. III A, we perform a symmetry reduction of Einstein equations to obtain a set of geometrical equations in the three-dimensional quotient manifold. These equations can be viewed as three-dimensional Einstein equations coupled with effective matter sources. In the second step (Sec. III B) we chose an arbitrary spacelike foliation in the quotient manifold and split the equations in time plus space. In Sec. III C we fix the foliation and the coordinate system. We also write the mass formula in this gauge. Finally, in Sec. III D we discuss boundary conditions at the axis and at infinity.

A. Symmetry reduction

In this section we perform the symmetry reduction of the field equations. We follow [2,16]. See also [5,14].

Consider a vacuum solution of Einstein's equations, i.e., a four-dimensional manifold M with metric $g_{\mu\nu}$ (with signature $(-+++)$) such that the corresponding Ricci tensor vanishes

$$^{(4)}\mathcal{R}_{\mu\nu} = 0. \tag{21}$$

Suppose, in addition, that the metric $g_{\mu\nu}$ admits a Killing field η^μ; that is η^μ satisfies the equation

$$\hat{\nabla}_{(\mu}\eta_{\nu)} = 0, \tag{22}$$

where $\hat{\nabla}_\mu$ is the connection with respect to $g_{\mu\nu}$. Greek indices $\mu, \nu, \cdots$ denote four-dimensional indices.

We define the square of the norm and the twist of η^μ, respectively, by

$$\eta = \eta^\mu \eta^\nu g_{\mu\nu}, \qquad \omega_\mu = \epsilon_{\mu\nu\lambda\gamma}\eta^\nu \hat{\nabla}^\lambda \eta^\gamma. \tag{23}$$

Using the field Eq. (21) it is possible to prove that

$$\hat{\nabla}_{[\mu}\omega_{\nu]} = 0, \tag{24}$$

and hence ω_μ is locally the gradient of a scalar field ω

$$\omega_\mu = \hat{\nabla}_\mu \omega. \tag{25}$$

Let $\mathcal{N}$ denote the collection of all trajectories of η^μ, and assume that it is a differential 3-manifold. We define the metric $h_{\mu\nu}$ on $\mathcal{N}$ by

$$\eta g_{\mu\nu} = h_{\mu\nu} + \eta_\mu \eta_\nu. \tag{26}$$

The vacuum field Eqs. (21) can be written in the following form on $\mathcal{N}$:

$$\Box\eta = \frac{1}{\eta}(\nabla^a \eta \nabla_a \eta - \nabla^a \omega \nabla_a \omega), \tag{27}$$

$$\Box\omega = \frac{2}{\eta}\nabla^a \omega \nabla_a \eta, \tag{28}$$

$$^{(3)}R_{ab} = \frac{1}{2\eta^2}(\nabla_a \eta \nabla_b \eta + \nabla_a \omega \nabla_b \omega), \tag{29}$$

where ∇_a and $^{(3)}R_{ab}$ are the connection and the Ricci

tensor of h_{ab}, we have defined $\Box = \nabla_a \nabla^a$, and Latin indices $a, b \ldots$ denote three-dimensional indices on $\mathcal{N}$.

Note that the definition of the metric (26) involves a conformal rescaling with respect to the canonical metric $\tilde{h}_{\nu\mu}$ defined by

$$g_{\nu\mu} = \tilde{h}_{\nu\mu} + \eta^{-1}\eta_\nu\eta_\mu. \tag{30}$$

That is, we have

$$h_{\mu\nu} = \eta\tilde{h}_{\mu\nu}. \tag{31}$$

This rescaling simplifies considerably the field equations. In particular, on the right-hand side of Eq. (29) there are no second derivatives of the fields η and ω (compare, for example, with Eq. (20) in [10]).

Finally, we note that Eq. (27) can be written in the following form:

$$\Box\Sigma = -\frac{\nabla^a\omega\nabla_a\omega}{\eta^2}, \tag{32}$$

where we have defined

$$\Sigma = \log\eta. \tag{33}$$

Up to this point, the only assumption we have made is that the spacetime admits a Killing vector field η^μ and that η^μ is not null, otherwise the metric h_{ab} is not defined. If the Killing field is timelike ($\eta < 0$) then the metric h_{ab} is Riemannian and the Eqs. (27)–(29) are the stationary Einstein vacuum equations. On the other hand, when the Killing vector is spacelike ($\eta > 0$), the metric h_{ab} is a is a three-dimensional Lorenzian metric (we chose the signature $(-++)$). In axial symmetry, the Killing vector η^μ is spacelike, and its norm vanishes at the axis of symmetry. Hence, the equations are formally singular at the axis. This singular behavior at the axis represents the main difficulty in handling these equations.

In the Lorenzian case, Eq. (29) has the form of Einstein equations in three dimensions, with effective matter sources produced by η and ω. The effective matter Eqs. (27) and (28) imply that the energy-momentum tensor defined in terms of η and ω by

$$T_{ab} = \frac{1}{2\eta^2}(\nabla_a\eta\nabla_b\eta + \nabla_a\omega\nabla_b\omega) - \frac{1}{4\eta^2}h_{ab}(\nabla_c\eta\nabla^c\eta + \nabla_c\omega\nabla^c\omega), \tag{34}$$

is divergence free, i.e. $\nabla^a T_{ab} = 0$.

A particularly relevant special case is when $\omega = 0$. In that case Eqs. (27) and (28) simplify considerably:

$$\Box\Sigma = 0, \tag{35}$$

$$^{(3)}R_{ab} = \frac{1}{2}\nabla_a\Sigma\nabla_b\Sigma. \tag{36}$$

We have pointed out that the rescaling (31) simplifies the equations and allows us to write them in a more geometric form. This is the reason why this scaling is used in the case of $U(1)$ cosmologies where the equations are locally the same but the norm η never vanishes (see [17,18] and the review article [19]). In our case the conformal scaling (31) is singular at the axis. However, since the behavior of η at the axis, as we will see in the next sections, is controlled *a priori* this singular scaling does not seem to introduce any extra difficulty in the equations. We also remark that in all the numerical works mentioned above this conformal rescaling was not used, and the equations are written in terms of the metric $\tilde{h}_{ab}$ defined by (30).

Equations (27)–(29) are purely geometric with respect to the metric h_{ab}. To solve these equations we need to prescribe some gauge for the metric h_{ab}. This will be done in the next two sections.

B. 2 + 1 decomposition

In order to formulate an initial value problem, we will perform an standard 2 + 1 decomposition of Eqs. (27)–(29). Note that this is completely analogous to the 3 + 1 decomposition of Einstein equations; in fact all the formulas are formally identical because the dimension does not appear explicitly in them (see, for example, [20], [21]).

Consider a foliation of spacelike, two-dimensional slices S of the metric h_{ab}. Let t be an associated time function and let n^a be the unit normal vector orthogonal to S with respect to the metric h_{ab}. The intrinsic metric on S is denoted by q_{ab} and is given by

$$h_{ab} = -n_a n_b + q_{ab}. \tag{37}$$

Define the density μ by

$$\mu = 2\,^{(3)}R_{ab}n^a n^b + {}^{(3)}R, \tag{38}$$

and the current J_b by

$$J_b = -q_b^c n^a\,^{(3)}R_{ca}, \tag{39}$$

where $^{(3)}R = {}^{(3)}R_{ab}h^{ab}$ denotes the trace of $^{(3)}R_{ab}$. Then, using Eq. (29) we obtain

$$\mu = \frac{1}{2\eta^2}(\eta'^2 + \omega'^2 + |D\eta|^2 + |D\omega|^2), \tag{40}$$

$$J_A = -\frac{1}{2\eta^2}(\eta' D_A\eta + \omega' D_A\omega), \tag{41}$$

where D_A is the connection with respect to q_{AB}. The prime denotes directional derivative with respect to n^a, that is

$$\eta' = n^a\nabla_a\eta = \frac{1}{\alpha}(\partial_t\eta - \beta^A D_A\eta) \tag{42}$$

where α is the lapse and β^A is the shift vector of the foliation. The indices $A, B, \cdots$ denote two-dimensional indices on S. The constraint equations corresponding to

(29) are given by

$$^{(2)}R - \chi^{AB}\chi_{AB} + \chi^2 = \mu, \tag{43}$$

$$D^A\chi_{AB} - D_B\chi = J_B, \tag{44}$$

where $^{(2)}R$ is the Ricci scalar of q_{AB}, χ_{AB} is the second fundamental form of S, and χ its trace

$$\chi = q^{AB}\chi_{AB}. \tag{45}$$

We use the following sign convention for the definition of χ_{AB}:

$$\chi_{ab} = -q_a^c\nabla_c n_b = -\frac{1}{2}\mathcal{L}_n q_{ab}, \tag{46}$$

where $\mathcal{L}$ denotes Lie derivative. The evolution equations are given by

$$\partial_t q_{AB} = -2\alpha\chi_{AB} + \mathcal{L}_\beta q_{AB}, \tag{47}$$

$$\partial_t\chi_{AB} = \mathcal{L}_\beta\chi_{AB} - D_A D_B\alpha + \alpha\tau_{AB}, \tag{48}$$

where

$$\tau_{AB} = \chi\chi_{AB} + {}^{(2)}R_{AB} - {}^{(3)}R_{AB} - 2\chi_{AC}\chi^C_B, \tag{49}$$

and

$$^{(3)}R_{AB} = \frac{1}{2\eta^2}(\partial_A\eta\partial_B\eta + \partial_A\omega\partial_B\omega). \tag{50}$$

The evolution Eqs. (47) and (48) and the constraint Eqs. (43) and (44) constitute a complete 2 + 1 decomposition of the three-dimensional Einstein Eq. (29). It remains to decompose the effective matter Eqs. (27) and (28). This can easily be obtained using the decomposition formula (A11) for the wave operator $\Box$ and the definition of the metric q_{ab} given by (37). The result is the following:

$$-\Sigma'' + \Delta_q\Sigma + D_A\Sigma\frac{D^A\alpha}{\alpha} + \Sigma'\chi = \frac{1}{\eta^2}(\omega'^2 - |D\omega|^2), \tag{51}$$

$$-\omega'' + \Delta_q\omega + D_A\omega\frac{D^A\alpha}{\alpha} + \omega'\chi = \frac{2}{\eta^2}(D_A\omega D^A\eta - \omega'\eta'), \tag{52}$$

where instead of (27) we have use (32), and Δ_q is the Laplacian with respect to q_{AB}, i.e. $\Delta_q = D^A D_A$.

Finally, we mention that the line element of the metric h_{ab} takes the standard form

$$h = -\alpha^2 dt^2 + q_{AB}(dx^A + \beta^A dt)(dx^B + \beta^B dt). \tag{53}$$

C. Gauge

In this section we describe the maximal-isothermal gauge. In particular we review the mass formula for this gauge (see [10] for details). For the lapse, we impose the maximal condition on the 2-surfaces

$$\chi = 0. \tag{54}$$

Note that we are not imposing that the surfaces are maximal in the three-dimensional picture as in [10]. The later condition is the one generally used [5,6], but the difference is only minor. In particular the mass formula is positive definite for both conditions as we will see. The one used here appears to be natural with respect to the rescaled metric h_{ab}. Equation (54) implies the following well-known equation for the lapse

$$\Delta_q\alpha = \alpha(\chi^{AB}\chi_{AB} + \mu_1), \tag{55}$$

where

$$\mu_1 = {}^{(3)}R_{ab}n^a n^b = \frac{1}{2\eta^2}(\eta'^2 + \omega'^2). \tag{56}$$

The maximal gauge (54) can be, of course, imposed in any dimension, and it is not related at all with axial symmetry. In contrast, the condition for the shift is peculiar for two space dimensions. The shift vector is fixed by the requirement that the intrinsic metric q_{AB} has the following form:

$$q_{AB} = e^{2u}\delta_{AB}, \tag{57}$$

where δ_{AB} is a fixed (i.e. $\partial_t\delta_{AB} = 0$) flat metric in two dimensions. Then, using (54), we obtain that the trace-free part of (47) is given by

$$2\alpha\chi_{AB} = (\mathcal{L}_q\beta)_{AB}, \tag{58}$$

where $\mathcal{L}_q$ is the conformal Killing operator in two dimensions with respect to the metric q_{AB} defined in Eq. (A1). Equation (58) is an elliptic first-order system of equations for β^A.

The elliptic Eqs. (55) and (58) determine lapse and shift for the metric h_{ab}, and hence they fix completely the gauge freedom in Eqs. (27)–(29). This gauge has associated a natural cylindrical coordinate system (t, ρ, z) for which the metric δ_{AB} is given

$$\delta = d\rho^2 + dz^2, \tag{59}$$

and the axis of symmetry is given by $\rho = 0$. The slices S are the half planes $\mathbb{R}^2_+$.

For the analysis of the equations it is of course important to write them explicitly as partial differential equations in these coordinates. We will do this in the remainder of this section. In general, due to the complexity of Einstein equations, the partial differential equations obtained in a particular gauge can be quite involved. In our case, however, the geometric nature of the gauge plus the symmetry reduction will provide a relatively simple set of equations.

We first present some useful definitions. We need to subtract from η the part that vanishes at the axis. We define the function σ by

$$\eta = \rho^2 e^{\sigma}. \tag{60}$$

Because of the rescaling (31), the lapse α vanishes also at the axis, hence we define the normalized lapse $\bar{\alpha}$ by

$$\alpha = \rho\bar{\alpha}. \tag{61}$$

From the regularity conditions presented in the next section we will see that it is useful to define the function q defined by

$$u = \log\rho + \sigma + q. \tag{62}$$

We now proceed to write the equations. We begin with the evolution equations for σ and ω. The evolution equation for σ is given by (51). Using the definition (60) and the conformal rescaling expression for the Laplacian (A6) we obtain

$$\begin{aligned} &- e^{2u}\sigma'' + {}^{(3)}\Delta\sigma + \partial_A\sigma\frac{\partial^A\bar{\alpha}}{\bar{\alpha}} - 2e^{2u}(\log\rho)'' + 2\frac{\partial_\rho\bar{\alpha}}{\bar{\alpha}\rho} \\ &= (-e^{2u}(\omega')^2 + |\partial\omega|^2)\rho^{-4}e^{-2\sigma}. \end{aligned} \tag{63}$$

In the same way, from (52) we get

$$\begin{aligned} &- e^{2u}\omega'' + {}^{(3)}\Delta\omega + \partial_A\omega\frac{\partial^A\bar{\alpha}}{\bar{\alpha}} \\ &= \frac{2}{\eta}(-e^{2u}\omega'\eta' + \partial_A\omega\partial^A\eta), \end{aligned} \tag{64}$$

where ∂_A denotes partial derivatives with respect to ρ and z and all the indices are moved with respect to the flat metric δ_{AB}. In these equations the lapse α and the shift β^A appear through the prime operator defined in (42).

The momentum constraint (44) is given by

$$\partial^B\chi_{AB} = \bar{J}_A, \tag{65}$$

where $\bar{J}_A = e^{2u}J_A$; that is we have

$$\bar{J}_A = -\frac{e^{2u}}{2\eta^2}(\eta'\partial_A\eta + \omega'\partial_A\omega). \tag{66}$$

To obtain (65) we have used the conformal rescaling of the divergence in two dimensions given by (A8). The indices in Eq. (65) and in the rest of the article are moved with the flat metric δ_{AB}. To avoid confusion, it is useful to introduce the following notation:

$$\begin{aligned} \hat{\beta}_A = \beta^A\delta_{AB}, \qquad \hat{\chi}^A_B = \delta^{AC}\chi_{CB}, \\ \hat{\chi}^{AB} = \delta^{AC}\delta^{BD}\chi_{CD}. \end{aligned} \tag{67}$$

That is, we want to distinguish between, say, the covector $\beta_A = \beta^B q_{AB}$ used in the previous section and $\hat{\beta}_A$ (see the discussion after Eq. (A10) in the Appendix).

The Hamiltonian constraint, Eq. (43), is given by

$${}^{(3)}\Delta\sigma + \Delta q = -\frac{\epsilon}{4}, \tag{68}$$

where

$$\epsilon = \frac{e^{2u}}{\eta^2}(\eta'^2 + \omega'^2) + |\partial\sigma|^2 + \frac{|\partial\omega|^2}{\eta^2} + 2e^{-2u}\hat{\chi}^{AB}\chi_{AB}. \tag{69}$$

Let us consider the evolution equations for q_{AB} and χ_{AB}. The evolution equation for the metric q_{AB} reduces to

$$2\partial_t u = \partial_A\beta^A + 2\beta^A\partial_A u. \tag{70}$$

And the evolution equation for the second fundamental form χ_{AB} is given by

$$\partial_t\chi_{AB} = \mathcal{L}_\beta\chi_{AB} - F_{AB} - \alpha G_{AB} - 2\alpha\chi_{AC}\hat{\chi}^C_B \tag{71}$$

where F_{AB} denotes the trace-free part (with respect to δ_{AB}) of $D_AD_B\alpha$. Using Eq. (A4)) we obtain

$$F_{AB} = \partial_A\partial_B\alpha - \frac{1}{2}\delta_{AB}\Delta\alpha - 2\partial_{(A}\alpha\partial_{B)}u + \partial_C\alpha\partial^C u\delta_{AB}. \tag{72}$$

And G_{AB} denotes the trace-free part of ${}^{(3)}R_{AB}$, namely

$$G_{AB} = {}^{(3)}R_{AB} - \frac{1}{2}\delta_{AB}{}^{(3)}R_{CD}\delta^{CD}, \tag{73}$$

where ${}^{(3)}R_{AB}$ is given by (50).

The equation for the lapse is given by

$$\Delta\alpha = \alpha(e^{-2u}\hat{\chi}^{AB}\chi_{AB} + e^{2u}\mu_1), \tag{74}$$

and for the shift we have

$$(\mathcal{L}\beta)^{AB} = 2\alpha e^{-2u}\hat{\chi}^{AB}, \tag{75}$$

where $\mathcal{L}$ is the flat conformal Killing operator defined by (A2).

Using the identity (A3), we can transform the first-order system of Eqs. (75) for the shift and for the momentum constraint (65) in a pair of second-order uncoupled equations. For the shift, we take a divergence to Eq. (75) to obtain

$$\Delta\beta^A = 2\partial_B(\alpha\hat{\chi}^{AB}e^{-2u}). \tag{76}$$

For Eq. (65) we define the vector v^A by

$$\chi_{AB} = \mathcal{L}(v)_{AB}, \tag{77}$$

and hence Eq. (75) transforms to

$$\Delta v_A = \bar{J}_A. \tag{78}$$

The total Arnowitt-Deser-Misner mass of the spacetime can be calculated as a volume integral on the half plane $\mathbb{R}^2_+$ of the positive definite effective energy density (66) (see [10])

$$m = \frac{1}{16}\int_{\mathbb{R}^2_+}\epsilon\rho d\rho dz. \tag{79}$$

Finally, we mention that in the twist-free case ($\omega = 0$) the four-dimensional spacetime metric $g_{\mu\nu}$ has a simple expression in these coordinates, namely

$$g = -\frac{\alpha^2}{\rho^2}e^{-\sigma}dt^2 + e^{\sigma+2q}((d\rho + \beta^\rho dt)^2 + (dz + \beta^z dt)^2) + \rho^2 e^{\sigma} d\phi^2. \quad (80)$$

D. Boundary conditions and axial regularity

The boundary conditions at the axis in axial symmetry have been widely analyzed in the literature [4,5,7,14]. They involve parity conditions in the ρ dependence for the different fields. That is, the relevant functions are either even or odd functions of ρ. In order to use these results in our setting, it is useful to write the relations of the quantities with respect to the rescaled metric h_{ab} and the canonical metric $\tilde{h}_{ab}$, since all the above-mentioned articles work with the metric $\tilde{h}_{ab}$.

Using relation (31) we obtain for the two-dimensional metric

$$q_{AB} = \eta \tilde{q}_{AB}, \quad (81)$$

and for the second fundamental form

$$\chi_{AB} = \sqrt{\eta}\left(\tilde{\chi}_{AB} + \frac{1}{2}\frac{\eta'}{\eta}\tilde{q}_{AB}\right), \quad (82)$$

where quantities with a tilde are written with respect to the metric $\tilde{h}_{ab}$. We also have

$$\alpha = \sqrt{\eta}\tilde{\alpha}, \qquad \beta^A = \tilde{\beta}^A. \quad (83)$$

Using these relations and the results mentioned above it is straightforward to obtain the following behavior of the relevant variables:

$$\eta, \omega, \bar{\alpha}, u, q, \sigma, \chi_{\rho\rho}, \beta^z \text{ are even functions of } \rho, \quad (84)$$

and

$$\chi_{\rho z}, \beta^\rho \text{ are odd functions of } \rho. \quad (85)$$

Note that odd functions vanish at the axis and the ρ derivative of even functions vanishes at the axis. It follows that one can impose homogeneous Dirichlet boundary conditions at the axis for odd functions and homogeneous Neumann boundary conditions for even functions. In addition, we have that the function q defined by (62) should vanish at the axis

$$q|_{\rho=0} = 0. \quad (86)$$

Since q is an even function, from (86) we deduce that $q = O(\rho^2)$ near the axis. Finally, there is an important regularity condition which comes from the axial regularity of the three-dimensional extrinsic curvature. Let us define the following quantity:

$$w = \frac{1}{\rho}\left(-\frac{\eta'}{\eta} + \chi_{\rho\rho}\right). \quad (87)$$

Then it follows that

$$w = O(\rho), \quad (88)$$

near the axis. This is the equivalent to the regularity condition given in Eq. (50) in [14] adapted to our conformally rescaled metric. See also [5,7].

The falloff conditions at infinity are the standard asymptotically flat ones. In particular we have

$$\lim_{r\to\infty} \bar{\alpha} = 1, \quad (89)$$

and

$$\sigma, \beta^A = O(r^{-1}), \qquad \chi_{AB} = O(r^{-2}), \quad (90)$$

as $r \to \infty$.

IV. LINEARIZED EQUATIONS

In this section we make a linear expansion around Minkowski of the Einstein equations in the maximal-isothermal gauge described in the previous section. Note that for Minkowski we have

$$\eta = \rho^2, \quad (91)$$

and hence, due to the rescaling (31), the background metric h_{ab}, given in coordinates by (53), is nonflat

$$h = \rho^2(-dt^2 + d\rho^2 + dz^2). \quad (92)$$

The other background quantities are given by

$$\omega = 0, \qquad \alpha = \rho, \qquad \beta^A = 0, \qquad \chi_{AB} = 0, \quad (93)$$

and

$$u = \ln\rho, \qquad q = 0, \qquad \sigma = 0. \quad (94)$$

The Hamiltonian constraint and the equation for the lapse are nontrivial for the metric (92), namely

$$\Delta\alpha = 0, \qquad \Delta u = \frac{2}{\rho^2}. \quad (95)$$

Let us proceed with the linearization. For simplicity we will consider only the case $\omega = 0$. The first step is to compute the lapse function. The right-hand side of Eq. (74) is second order, then, using the boundary condition (89) we obtain

$$\bar{\alpha} = 1. \quad (96)$$

That is, the maximal condition for the lapse is trivial at the linearized level. On the contrary, as we will see, the equation for the shift plays a crucial role.

The next step is to compute the linearization of the wave Eq. (63) for σ; we obtain

$$-\dot{p} + {}^{(3)}\Delta\sigma = 0, \quad (97)$$

where a dot means a partial derivative with respect to t and we have defined

$$p = \dot{\sigma} - \frac{2\beta^{\rho}}{\rho}. \tag{98}$$

In order to close the system we need an equation for β^{ρ}. Using Eqs. (65) and (66) for the momentum we obtain

$$\partial^{A}\chi_{AB} = \bar{J}_{A}, \tag{99}$$

with

$$\bar{J}_{A} = -p\partial_{A}\rho. \tag{100}$$

We define the vector field v^{A} by Eq. (77) and then by Eq. (78) we obtain

$$\Delta v_{A} = -p\partial_{A}\rho. \tag{101}$$

From (100) we deduce $J_{z} = 0$ and hence we get

$$\Delta v_{z} = 0. \tag{102}$$

By the falloff condition (90), we obtain

$$v_{z} = 0. \tag{103}$$

In the following, to simplify the notation we set

$$v \equiv v_{\rho}. \tag{104}$$

Equation (101) reads

$$\Delta v = -p. \tag{105}$$

Using (77) we also obtain

$$\chi_{\rho\rho} = \partial_{\rho} v, \qquad \chi_{\rho z} = \partial_{z} v. \tag{106}$$

For the shift we have the equation

$$(\mathcal{L}\beta)^{AB} = 2\frac{\hat{\chi}^{AB}}{\rho}. \tag{107}$$

Taking a divergence to this equation (or linearizing (76)) we obtain

$$\Delta\beta^{A} = 2\partial_{B}\left(\frac{\hat{\chi}^{AB}}{\rho}\right). \tag{108}$$

Note that in (108) we get an equation for β^{ρ} decoupled from β^{z}. Using Eqs. (99) and (100) from this equation we get

$$\Delta\beta^{\rho} = -\frac{2}{\rho}\left(p + \frac{\partial_{\rho} v}{\rho}\right). \tag{109}$$

Equation (109) together with (97) and (105) form a complete system for the variables v, σ, and β^{ρ}. Alternatively, using Eqs. (99) and (107) we can eliminate χ_{AB} and hence also v. We get the following equation for β^{A}:

$$\partial_{B}(\rho(\mathcal{L}\beta)^{AB}) = -2p\partial^{A}\rho. \tag{110}$$

Equation (110) together with (97) and (105) form a complete system for the variables σ, β^{ρ}, and β^{z}.

There is however an important difficulty. The linearization of the regularity condition (87) and (88) is given by

$$w = -\frac{1}{\rho}\left(p + \frac{\partial_{\rho} v}{\rho}\right), \qquad w = O(\rho), \tag{111}$$

where we have used Eq. (106). From the set of equations presented above, it is difficult to ensure that this condition will be satisfied. To enforce this condition we will write the equations in terms of different variables. In order to do that, we need first to compute the remaining equations, namely, the Hamiltonian constraint and the evolution equations for the metric and second fundamental form. Since ϵ defined in (69) is second order, the Hamiltonian constraint (68) is given by

$$\Delta q = -{}^{(3)}\Delta\sigma. \tag{112}$$

The evolution equation for q is obtained from (70)

$$\dot{q} + \dot{\sigma} = \frac{1}{2}\partial_{A}\beta^{A} + \frac{\bar{\beta}^{\rho}}{\rho}. \tag{113}$$

The evolution equation for χ_{AB} is obtained linearizing (71)

$$\dot{\chi}_{AB} = 2\partial_{(A}q\partial_{B)}\rho - \delta_{AB}\partial_{\rho} q. \tag{114}$$

We can also write the evolution Eqs. (114) in components

$$\dot{\chi}_{\rho\rho} = \partial_{\rho} q, \qquad \dot{\chi}_{\rho z} = \partial_{z} q. \tag{115}$$

Using Eqs. (106) we deduce the important relation

$$\dot{v} = q, \tag{116}$$

which holds only in the twist-free case. This relation simplifies the equations considerably. From Eq. (114) we also deduce

$$\partial^{B}\dot{\chi}_{AB} = \Delta q\partial_{A}\rho. \tag{117}$$

With these equations we can compute the time derivative of w

$$\dot{w} = \frac{1}{\rho}\left(\Delta q - \frac{\partial_{\rho} q}{\rho}\right), \tag{118}$$

and hence the evolution equation for q is given by

$$\dot{q} = \rho w + \rho\partial_{\rho}\left(\frac{\beta^{\rho}}{\rho}\right). \tag{119}$$

As a consequence, q satisfies the following wave equation:

$$\ddot{q} = \Delta q - \frac{\partial_{\rho} q}{\rho} + \rho\partial_{\rho}\left(\frac{\dot{\beta}^{\rho}}{\rho}\right). \tag{120}$$

We also have

$$\Delta\dot{\beta}^{\rho} = \frac{2}{\rho}\left(\Delta q - \frac{\partial_{\rho} q}{\rho}\right). \tag{121}$$

Equations (120) and (121) form a complete system for the variables q and β^{ρ}. A similar choice of variable was used by [4–6]. However, in our particular case (i.e. linear equation without twist) it is possible a further simplification, namely to use Eq. (116) and hence replace q by $v$in these

equations and then integrate in time. In this way we obtain our main Eqs. (1) and (2). The advantage of using υ as a variable is that the mass integral has a simple expression in terms of υ given by (19). This formula for the mass is obtained expanding up to second order the energy density (69), using Eqs. (106) to replace χ_{AB} and Eq. (105) to replace η'/η. We discuss this in more detail in the next section.

The boundary conditions (4) and (5) for β^ρ arise from the axial regularity condition (85) and the asymptotically flat falloff (90). Conditions (8) arise from the axial regularity conditions for q given by (84) and (86). The main advantage of Eqs. (1) and (2) is that they have built in the regularity condition (111) as we will see in the next section. Let us mention that the nontrivial regularity condition (111) is written in terms of υ as follows:

$$w = \frac{1}{\rho}\left(\Delta\upsilon - \frac{\partial_\rho \upsilon}{\rho}\right), \qquad w = O(\rho). \tag{122}$$

The component β^z, which does not appear in Eqs. (1) and (2), can be calculated using

$$\partial_\rho \beta^\rho - \partial_z \beta^z = 2\frac{\partial_\rho \upsilon}{\rho}, \tag{123}$$

$$\partial_z \beta^\rho + \partial_\rho \beta^z = 2\frac{\partial_z \upsilon}{\rho}, \tag{124}$$

or, alternatively, using Eq. (16) which is obtained taking a derivative to Eqs. (123) and (124). Finally, the four-dimensional perturbation (10) is obtained using the line element (80) and the background values (91), (93), and (94).

V. PROPERTIES OF THE LINEAR EQUATIONS

In this section we analyze some properties of our linear Eqs. (1) and (2). We begin with the symmetries of these equations. The first symmetry is given by translation in z. This is to be expected since the gauge fixes the axis (and hence there is no translation freedom in ρ), but we still have the freedom to chose the origin in the z coordinate. Then, if we have a solution υ, β^ρ; the derivative $\partial_z\upsilon$, $\partial_z\beta^\rho$ is also a solution, since ∂_z commute with all the differential operators because their coefficients depend only on ρ. The same argument applies to time translations, which is the second symmetry of the equations. The third symmetry is scaling. Let s be a positive real number. For a given solution $\upsilon(t, \rho, z)$ we define the rescaled function as

$$\upsilon_s(\hat{t}, \hat{\rho}, \hat{z}) = \upsilon\left(\frac{t}{s}, \frac{\rho}{s}, \frac{z}{s}\right), \tag{125}$$

where

$$\hat{t} = \frac{t}{s}, \qquad \hat{\rho} = \frac{\rho}{s}, \qquad \hat{z} = \frac{z}{s}, \tag{126}$$

and the same for β^ρ. Then, υ_s define also a solution in terms of the rescaled coordinates. The mass rescales like

$$m \to sm. \tag{127}$$

In order to understand the equations in a simple situation, let us first consider Eqs. (1) and (2) on a bounded domain Ω which does not contain the axis. On Ω the coefficient of Eqs. (1) and (2) are smooth. Equation (2) is an elliptic equation for β^ρ if we consider υ as a given function. Hence, in order to solve this equation we need to prescribe elliptic boundary conditions for β^ρ on $\partial\Omega$, for example, Dirichlet or Neumann boundary conditions. Equation (1) is a wave equation for υ if we consider β^ρ as a given function. To solve this wave equation we need to prescribe initial data for υ and $\dot{\upsilon}$ at $t = 0$ together with compatible boundary conditions for υ at $\partial\Omega$. For example Dirichlet, Neumann, or Sommerfeld boundary conditions for υ at $\partial\Omega$. The equations are of course coupled, so it is not obvious that the above procedure of fixing boundary conditions is correct since υ and β^ρ are not "given functions." However, it is possible to prove that this is procedure is in fact correct. Consider the following iteration scheme:

$$\ddot{\upsilon}_{n+1} - \Delta\upsilon_{n+1} + \frac{\partial_\rho \upsilon_{n+1}}{\rho} = \rho\partial_\rho\left(\frac{\beta^\rho_n}{\rho}\right), \tag{128}$$

$$\Delta\beta^\rho_{n+1} = \frac{2}{\rho}\left(\Delta\upsilon_n - \frac{\partial_\rho \upsilon_n}{\rho}\right). \tag{129}$$

In this iteration, the equations are not coupled, and hence the boundary conditions mentioned above (which are kept fixed) are correct. Following similar arguments to the one presented in [22] (see also [23]) it is not difficult to see that this iteration converges for some small time interval. And hence we get well-posedness for the linear system (1) and (2) under these boundary conditions on the domain Ω. The reason why the iteration (128) and (129) converges is the following. From Eq. (129), using standard elliptic, estimates we obtain that β^ρ is equivalent (in number of derivatives) to υ. Hence, the term containing β^ρ in Eq. (128) is equivalent to a first-order derivative of υ, and then it is not in the principal part of the wave equation. This rough argument suggests that the combination of elliptic estimates and energy estimates for the wave equations will close and hence the iteration will converge. This is basically the argument presented in [22,23]. If the domain Ω is not bounded, this argument will still work if we add appropriate falloff conditions at infinity. However, the situation changes drastically when Ω includes the axis. Let us analyze that case.

Since the axis is a singular boundary for the equations, we are not free to chose an arbitrary boundary condition there. In fact β^ρ and $\partial_\rho\upsilon$ should vanish at the axis, otherwise the equations become singular. If we use L'Hôpital rule, we conclude that the term with β^ρ in (1) contains in fact two derivatives with respect to ρ at the axis. That is,

due to the L'Hopital limit, to divide by ρ is equivalent as to take a derivative with respect to ρ at the axis. But then, using Eq. (2), we conclude that this term is equivalent to second derivatives of v and hence it is in the principal part of the wave equation. We ccannot conclude that the iteration scheme (128) and (129) converges if we include the axis in the domain. This is, roughly speaking, the main difficulty to prove the well-posedness of the linear system (1) and (2). It appears to be difficult to identify the principal part of the system at the axis and to construct an appropriate iteration scheme.

Let us discuss in detail the boundary conditions at the axis. We are interested in solutions v which vanish at the axis; this comes from the regularity condition (86). Moreover, we have seen in Sec. III D that the smoothness of the spacetime metric at the axis implies that the functions β^ρ and v should satisfy the parity conditions (84) and (85). Let us see heuristically how these conditions are automatically implied by the equations provided we impose the following standard boundary conditions. At the axis we impose

$$\beta^\rho|_{\rho=0} = 0. \tag{130}$$

For v we prescribe initial data

$$v|_{t=0} = f, \qquad \dot{v}|_{t=0} = g, \tag{131}$$

such that

$$f|_{\rho=0} = 0, \qquad g|_{\rho=0} = 0. \tag{132}$$

Note that we are not imposing any condition on v at the axis for $t > 0$. We make a formal series expansion, namely, let as assume that our solution is smooth at the axis and has the form

$$v = \sum_{n=0}^{\infty} \rho^n a_n(t, z), \qquad \beta^\rho = \sum_{n=0}^{\infty} \rho^n b_n(t, z). \tag{133}$$

Substituting these expansions in Eqs. (1) and (2) we obtain the following recurrence relation for the coefficients:

$$\ddot{a}_n = (n+2)na_{n+2} + \partial_z^2 a_n + nb_{n+1}, \tag{134}$$

and

$$(n+1)nb_{n+1} + \partial_z^2 b_{n-1} = 2(n+2)na_{n+2} + \partial_z^2 a_n. \tag{135}$$

These expressions are valid for all integer n, with the convention that the coefficients b_n and a_n vanished for $n < 0$. The first nontrivial n in Eq. (134) is $n = -1$, which gives the relation

$$a_1 + b_0 = 0. \tag{136}$$

The term $n = 0$ is given by

$$\ddot{a}_0 = \partial_z^2 a_0. \tag{137}$$

This is a wave equation in one dimension. From the boundary conditions (130) we obtain

$$b_0 = 0. \tag{138}$$

Hence we deduce from (136) that

$$a_1 = 0. \tag{139}$$

From the initial data conditions (132) we have that

$$a_0|_{t=0} = 0, \qquad \dot{a}_0|_{t=0} = 0. \tag{140}$$

These provides trivial initial data for the wave Eq. (137) and hence we deduce

$$a_0 = 0. \tag{141}$$

That is, we have deduced the behavior $v = O(\rho^2)$ only from the boundary conditions (130) and the condition on the initial data (131). We want to prove now that (138) and (139) imply that all a_n with n odd and all b_n with n even are zero. We prove this by induction. Let us assume that for some n (with $n \geq 1$) we have that

$$b_{n-1} = 0, \qquad a_n = 0. \tag{142}$$

Using Eq. (135) we deduce

$$(n+1)b_{n+1} = 2(n+2)a_{n+2}, \tag{143}$$

and from (134) we have

$$(n+2)a_{n+2} = -b_{n+1}. \tag{144}$$

And then we have $a_{n+2} = b_{n+1} = 0$. Since (142) is valid for $n = 1$ we have proven the desired result. That is, the solutions v and β^ρ satisfy the parity conditions (84) and (85) respectively. Using that v is an even function of ρ and that $v = O(\rho^2)$ it is straightforward to deduce that the regularity condition (122) holds for all times.

We analyze now the falloff behavior of the solution v. This behavior is completely determined by the initial data f and g. Let us assume that the initial data have compact support. In the case of the wave equation, the signal will propagate with finite speed and hence the solution will always have compact support for any finite time. In our case, however, the coupling with the elliptic Eq. (2) produces a nonlocal behavior. Even if we start with compactly supported data, the function β^ρ will instantaneously spread to all space. Let us perform a formal expansion in r to see the typical behavior of v. We have that $\beta^\rho = O(r^{-1})$ for all times; this is prescribed by the boundary conditions. In [10] it has been proven that this implies that $\beta^\rho/\rho = O(r^{-2})$, and hence the terms containing β^ρ in (1) are $O(r^{-2})$. Then, at $t = 0$ we obtain that $\ddot{v} = O(r^{-2})$. If we take time derivatives of the equations and repeat this argument, we get that all time derivatives of v are $O(r^{-2})$. Then, we conclude that the typical falloff behavior for asymptotically flat solutions is given by (9), in the sense that we cannot expect a faster decay in general. Instead of compactly supported data we can begin with initial data for v such that they are $O(r^{-2})$ at infinity.

Let us discuss now the most important property of Eqs. (1) and (2), namely, the mass conservation. As usual, the mass appears as a second-order quantity that can be calculated in terms of squares of first-order quantities. The density (69) up to this order is given

$$\epsilon = 4\frac{|\partial v|^2}{\rho^2} + (\Delta v)^2 + |\partial\sigma|^2. \tag{145}$$

The total mass is calculated by the integral (79). The mass integral is conserved for the full nonlinear equations in this gauge (see [10]) and hence it is conserved at the linearized level. It is however important to compute explicitly this conservation formula using only the linear Eqs. (1) and (2). Note that the function σ appears in the mass and this function should be calculated from v using Eq. (12). To compute the time derivative of m we need first to calculate the time derivative of σ. Using the evolution Eq. (1) only, we compute

$${}^{(3)}\Delta\left(-\Delta v + 2\frac{\beta^\rho}{\rho}\right) = -\Delta\dot{v} + \frac{1}{\rho}\partial_\rho[\rho(\Delta\beta^\rho - 2L(v))], \tag{146}$$

where we have defined

$$L(v) = \partial^A\left(\frac{\partial_A v}{\rho}\right) = \frac{1}{\rho}\left(\Delta v - \frac{\partial_\rho v}{\rho}\right). \tag{147}$$

Then, using (2) and the time derivative of (12) we get

$${}^{(3)}\Delta\left(-\Delta v + 2\frac{\beta^\rho}{\rho} - \dot{\sigma}\right) = 0. \tag{148}$$

If we are solving in the whole half plane $\mathbb{R}^2_+$ then, by the falloff conditions, we deduce that the only possible solution of this equation is the trivial one, and hence

$$\dot{\sigma} = -\Delta v + 2\frac{\beta^\rho}{\rho}. \tag{149}$$

We have proven that Eqs. (1) and (2) together with (12) imply Eq. (149). We can also formulate the system in a different way. We can take (1) and (2) and Eq. (149), instead of (12), as an evolution equation for σ. If we take the Laplacian ${}^{(3)}\Delta$ to both sides of Eq. (146) and use the identity (142) together with Eq. (2) we obtain

$${}^{(3)}\Delta\dot{\sigma} = -\Delta\ddot{v}. \tag{150}$$

Hence, if we chose initial condition for σ such that

$${}^{(3)}\Delta\sigma|_{t=0} = -\Delta\dot{v}|_{t=0}, \tag{151}$$

Equation (150) implies (12). This two different ways of calculating σ correspond to a constrained system and a free system (using the terminology defined in [7]). The previous calculation is nothing but the propagation of the Hamiltonian constraint at the linearized level. For the full Einstein equations, the difference of constrained and free evolution schemes involves different set of evolutions equations. In our linear system the evolution equations are the same (namely, (1) and (2)), the difference is the way the function σ (and hence the mass) is calculated. These two ways are of course completely equivalent when the domain is the whole half plane $\mathbb{R}^2_+$, however, as we will see, they are not equivalent for a bounded domain.

Using Eqs. (1), (2), (12), and (149) we obtain the following local conservation law for the density ϵ defined by (145):

$$\rho\dot{\epsilon} = \partial_A\epsilon^A, \tag{152}$$

where

$$\epsilon_A = 8\frac{\partial_A v}{\rho}\dot{v} + 2\rho\dot{\sigma}\partial_A\sigma + 4\beta^\rho\partial_A\dot{v} - 4\dot{v}\partial_A\beta^\rho. \tag{153}$$

The vector ϵ^A can be interpreted as the energy flow of the gravitational field. If we integrate Eq. (152) in $\mathbb{R}^2_+$ we have that the boundary terms vanish both at the axis (by the axial regularity) and at infinity (by the falloff conditions). Then we have

$$\dot{m} = 0. \tag{154}$$

We can also integrate Eq. (152) on a bounded domain Ω, namely, we define the mass contained in Ω by

$$m_\Omega = \int_\Omega \epsilon\rho d\rho dz, \tag{155}$$

and then we have

$$\dot{m}_\Omega = \oint_{\partial\Omega} \epsilon^A n_A, \tag{156}$$

where n^A is the unit normal of $\partial\Omega$. The quantity $\epsilon^A n_A$ measures how much energy is leaving or entering the domain. The local conservation formula (152) can be generalized for the nonlinear equations [24].

Using the conservation of the mass (154) we can prove uniqueness of solutions of the system. Let us say we have two different solutions with the same initial data. We take the difference between the two solutions. The difference satisfies the same equation with zero initial data. In particular σ on the initial surface is zero. And hence the mass is zero. Since it is conserved the mass is zero for all times, which implies that the solution is zero.

In the case of hyperbolic equations (the wave equation, for example) the conservation of the energy gives also local properties of the solution, namely, finite speed propagation of signals. However this is not the case here; the elliptic equation implies a nonlocal behavior of the solution.

The discussion above applies for the domain $\mathbb{R}^2_+$, which is the relevant domain for the equations. However, in numerical computation we need to solve the equations on a finite grid and hence it is necessary to impose boundary conditions on a bounded domain. A typical domain for the numerics is shown in Fig. 1. As we mention in Sec. II, for our present purpose we only need to prescribe some bound-

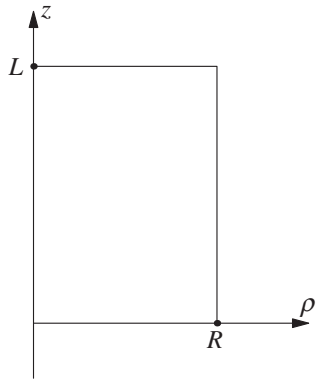

FIG. 1. The bounded domain Ω for the numerical evolution.

ary conditions compatible with asymptotic flatness. For example, homogeneous Dirichlet boundary conditions for υ and β^ρ. However, the mass formula raises an interesting point here. On a bounded domain, to calculate σ we have two possibilities. First, we can determine σ as the unique solution of the elliptic Eq. (12) with some boundary conditions. If we do so, then we again deduce Eq. (148). However, from this equation we cannot deduce (149). In effect, we have

$$\dot{\sigma} + \Delta\upsilon - 2\frac{\beta^\rho}{\rho} = H, \tag{157}$$

where H satisfies

$$^{(3)}\Delta H = 0. \tag{158}$$

We cannot conclude that H is zero from this equation, because H will have a nontrivial boundary condition. Namely, let us assume that we prescribe some boundary condition for σ. We cannot control the boundary value of $\Delta\upsilon$, and hence we cannot ensure that H vanishes at the boundary. In fact, the function H is fixed as the unique solution of (158) with boundary values

$$H|_{\partial\Omega} = \left(\dot{\sigma} + \Delta\upsilon - 2\frac{\beta^\rho}{\rho}\right)\Big|_{\partial\Omega}. \tag{159}$$

Then, if we compute the time derivative of the density ϵ we get

$$\rho\dot{\epsilon} = \partial_A\epsilon^A + \rho H\Delta\dot{\upsilon}. \tag{160}$$

That is, we do not get a conservation law; there is a volume term given by H. There seems to be no boundary conditions for σ that can ensure H vanishes.

The other possibility is to compute σ using the evolution Eq. (149) with initial condition (151). From (149), in the same way as we mentioned above we deduce (150), since in this deduction the boundary conditions play no role. Using the initial data condition (151), from (150) we deduce (12). That is, we are in the same situation as the whole domain. Hence, in this case we recover (152), where ϵ^A is given by the same expression (153). From this point of view, this evolution scheme appears to be better than the previous one.

In this scheme, we are free to chose any elliptic boundary condition for β^ρ and any boundary condition for υ compatible with the wave equation. For σ we do not have any freedom, and hence we cannot prescribe the boundary value of this function.

A natural choice of boundary conditions would be to force the boundary integral in (156) to have a definite sign. These conditions would have the interpretation of radiative boundary conditions, in the sense that the energy is leaving the domain. To prescribe such conditions seems not to be possible (at least for generic data) since we do not have any control on the term with σ. However, we can do something intermediate. Namely, if we impose Sommerfeld boundary condition for υ

$$\dot{\upsilon} = -n^A\partial_A\upsilon, \tag{161}$$

and homogeneous Dirichlet conditions for β^ρ we have that the first term in (163) has negative sign, and the third term is zero. For the second and fourth term we have no control *a priori*. But we can expect that the influence of these terms is small at least for some class of initial data. If this is true, then we get

$$\dot{m}_\Omega \leq 0. \tag{162}$$

This is what we observe in our numerical simulations described in the next sections.

VI. NUMERICAL IMPLEMENTATION

In this section we want to study numerically the initial-boundary value problem (IBVP) for Eqs. (1) and (2). In this problem the symmetry axis, $\rho = 0$, becomes a boundary of our domain. Notice then, that working with the variable υ poses an inconvenience as regards the boundary condition at $\rho = 0$ since, according to (8), this function satisfies both the homogeneous Dirichlet boundary condition and homogeneous Neumann boundary condition. It is then convenient to rewrite the equations in terms of a new variable for which the smoothness properties at the symmetry axis define a unique, equivalent, boundary condition. We define $\bar{\upsilon} = \upsilon/\rho$. This new variable vanishes linearly with ρ and the correct boundary condition is simply a homogeneous Dirichlet at $\rho = 0$.

The equation for $\bar{\upsilon}(\rho, z, t)$, with $\rho \in [0, R]$, $z \in [0, L]$, and $t \geq 0$, is

$$\ddot{\bar{\upsilon}} = \Delta\bar{\upsilon} + \partial_\rho\left(\frac{\bar{\upsilon}}{\rho}\right) + \partial_\rho\left(\frac{\beta^\rho}{\rho}\right), \tag{163}$$

where $\beta^\rho(\rho, z, t)$ is determined by the elliptic equation

$$\Delta\beta^\rho = 2\left(\Delta\bar{\upsilon} + \partial_\rho\left(\frac{\bar{\upsilon}}{\rho}\right)\right), \tag{164}$$

with homogeneous Dirichlet boundary conditions,

$$\begin{aligned}\beta^\rho(0,z,t) &= \beta^\rho(R,z,t) = 0, \qquad z \in [0,L],\\ \beta^\rho(\rho,0,t) &= \beta^\rho(\rho,L,t) = 0, \qquad \rho \in [0,R],\end{aligned} \tag{165}$$

for all $t \in [0,\infty)$.

The boundary condition for $\bar{v}$ at the symmetry axis is

$$\bar{v}(0,z,t) = 0, \tag{166}$$

while at the outer boundaries we study two possibilities, homogeneous Dirichlet,

$$\bar{v}(R,z,t) = \bar{v}(\rho,0,t) = \bar{v}(\rho,L,t) = 0, \tag{167}$$

or Sommerfeld (outgoing waves)

$$\begin{aligned}\dot{\bar{v}}(R,z,t) &= -\partial_\rho \bar{v}(R,z,t),\\ \dot{\bar{v}}(\rho,0,t) &= \bar{v}_z(\rho,0,t),\\ \dot{\bar{v}}(\rho,L,t) &= -\bar{v}_z(\rho,L,t).\end{aligned} \tag{168}$$

The initial data are

$$\bar{v}(\rho,z,0) = \bar{v}_0(\rho,z), \qquad \dot{\bar{v}}(\rho,z,0) = \bar{v}_{0t}(\rho,z), \tag{169}$$

where $\bar{v}_0$ and $\bar{v}_{0t}$ are C^∞ functions with compact support in $(0,R)\times(0,L)$ so that the compatibility of the boundary and initial data is not an issue.

The Eqs. (163)–(169) constitute the IBVP we approximate with our finite difference scheme.

We want to emphasize here an important difference between our numerical approach with the usual approaches in the area (see for example [5]). We solve the IBVP for (163) as a second-order equation just as it is written above, i.e. we do not reduce (163) to a first-order system of equations. The treatment of evolution equations as second-order equations as opposed to first-order systems of equations has several advantages. For example, the number of dynamical fields, and then the number of equations, is not increased. This facilitates the treatment of the boundary conditions. There are also numerical accuracy advantages. In the context of general relativity, this has been stressed in [25]. In particular the simplest proofs of well-posedness for general initial-boundary value problems for Einstein's equations have been found recently using second-order systems of equations [26,27].

a. The Implementation. In our numerical experiments we always consider square domains, i.e., $R = L$. To define the numerical grid let N be a positive integer and $h = L/N$ the space stepsize. We define our grid to be half a stepsize displaced from all the boundaries. We think of our grid as a uniformly distributed set of points each of which is at the center of one of the N^2 square cells covering the domain. The coordinates of the gridpoint at the site (i,k) are then

$$\rho_i = h(i-3/2), \qquad i = 0,1,2,\ldots N+3, \tag{170}$$

$$z_k = h(k-3/2), \qquad k = 0,1,2,\ldots N+3. \tag{171}$$

The sites (i,k) with $2 \le i,k \le N+1$ are within the domain, while the sites with $i = 0, 1, N+2, N+3$ and $k = 0, 1, N+2, N+3$ are "ghost points" used to ease the implementation of the boundary conditions [7]. Time is discretized as

$$t_n = n\delta t, \qquad n = 0,1,2,3,\ldots \tag{172}$$

We use capital Latin letters to denote the grid functions associated to the dynamical variables. Also, we use subindices to denote the space-site indices and a superindex to denote the time step. This is,

$$\begin{aligned}V^n_{i,k} &\text{ corresponds to } \bar{v}(\rho_i,z_k,t_n),\\ B^n_{i,k} &\text{ corresponds to } \beta^\rho(\rho_i,z_k,t_n).\end{aligned} \tag{173}$$

Besides the uniform grid we introduce the extra gridpoints placed at the physical boundary

$$(\rho = L, z_k), \qquad (\rho_i, z = 0), \qquad (\rho_i, z = L)$$

and denote the values of $\bar{v}$ at these points as

$$\bar{V}^{\,n}_{L,i}, \qquad \bar{V}^n_{i,0}, \qquad \bar{V}^n_{i,L}, \tag{174}$$

respectively.

In our difference scheme we approximate space derivatives by the standard fourth-order accurate centered difference operators given by [28]

$$\begin{aligned}D &:= D_0\left(I - \frac{h}{6}D_+D_-\right),\\ D^2 &:= D_+D_-\left(I - \frac{h^2}{12}D_+D_-\right),\end{aligned} \tag{175}$$

and add a subindex ρ or z to indicate what coordinate the operator is acting on. For example $\partial_z^2\bar{v}(\rho_i,z_k,t_n)$ is approximated by

$$D_z^2 V^n_{i,k} = \frac{-V^n_{i,k-2} + 16V^n_{i,k-1} - 30V^n_{i,k} + 16V^n_{i,k+1} - V^n_{i,k+2}}{12h^2}.$$

At every time step we need to solve the elliptic Eq. (164) which we approximate by

$$(D_\rho^2 + D_z^2)B^n_{i,k} = 2\left((D_\rho^2 + D_z^2)V^n_{i,k} + D_\rho\left(\frac{V^n_{i,k}}{\rho_i}\right)\right), \qquad i,k = 2,3,\ldots N+1. \tag{176}$$

We solve this difference equation iteratively using the Gauss-Seidel iteration scheme, and stop the iteration when the difference between both sides in (176) is smaller, in maximum norm, than a given small tolerance ε. We then extend the solution to the ghost points—so that the homogeneous boundary condition is satisfied—as follows:

$$\begin{aligned}&B^n_{0,k} = -B^n_{3,k}, \quad B^n_{1,k} = -B^n_{2,k}, \quad B^n_{N+2,k} = -B^n_{N+1,k},\\ &B^n_{N+3,k} = -B^n_{N,k}, \quad B^n_{i,0} = -B^n_{i,3}, \quad B^n_{i,1} = -B^n_{i,2},\\ &B^n_{i,N+2} = -B^n_{i,N+1}, \quad B^n_{i,N+3} = -B^n_{i,N}.\end{aligned}$$

We now describe how we approximate (163) using fourth-order accurate difference approximations in space;

to use second-order accurate approximations instead, we just need to change D and D^2 in what follows by D_0 and D_+D_- respectively.

$\underline{t=0}$. We set

$$V^0_{i,k} = \bar{v}_0(\rho_i, z_k), \qquad i,k = 2,3,\ldots N+1 \tag{177}$$

and extend the solution to vanish at all ghost points and boundary points since the initial data has compact support. Then we compute $B^0_{i,k}$ by solving (176) as explained above.

$\underline{t=\delta t}$ (first step). We do, for $i,\ k = 2,3,\ldots N+1$,

$$V^1_{i,k} = V^0_{i,k} + \delta t \bar{v}_{0t}(\rho_i, z_k) + \frac{1}{2}(\delta t)^2((D^2_\rho + D^2_z)V^0_{i,k} + D_\rho(V^0_{i,k}/\rho_i) + D_\rho(B^0_{i,k}/\rho_i)). \tag{178}$$

Now, if working with boundary condition (166) and (167), we define the solution at the boundary points to vanish

$$\bar{V}^{\,1}_{L,k} = \bar{V}^1_{i,0} = \bar{V}^1_{i,L} = 0, \tag{179}$$

while if working with boundary condition (166) and (168) we evolve the boundary points by integrating the boundary condition using an explicit Euler scheme. For example for the boundary $\rho = L$

$$\bar{V}^{\,1}_{L,k} = \bar{V}^0_{L,k} - \delta t \tilde{D}^\rho \bar{V}^0_{L,k}, \tag{180}$$

where

$$\tilde{D}^{\,\rho}\bar{V}^0_{L,k} = \frac{27(V^0_{N+2,k} - V^0_{N+1,k}) - (V^0_{N+3,k} - V^0_{N,k})}{24h}$$

is a fourth-order accurate approximation of the normal first derivative at the border $\rho = L$. We now extend the solution to the ghost points as

$$\begin{aligned} V^1_{0,k} &= -V^1_{3,k}, & V^1_{1,k} &= -V^1_{2,k} \\ V^1_{N+2,k} &= 2\bar{V}^1_{L,k} - V^1_{N+1,k}, & V^1_{N+3,k} &= 2\bar{V}^1_{L,k} - V^1_{N,k} \\ V^1_{i,0} &= 2\bar{V}^1_{i,0} - V^1_{i,3}, & V^1_{i,1} &= 2\bar{V}^1_{i,0} - V^1_{i,2} \\ V^1_{i,N+2} &= 2\bar{V}^1_{i,L} - V^1_{i,N+1}, & V^1_{i,N+3} &= 2\bar{V}^1_{i,L} - V^1_{i,N}. \end{aligned}$$

Finally, we compute $B^1_{i,k}$ as explained above.

At $\underline{t = n\delta t}$. With $n = 2,3,\ldots$ we evolve the solution with the two-step method

$$V^n_{i,k} = 2V^{n-1}_{i,k} - V^{n-2}_{i,k} + (\delta t)^2((D^2_\rho + D^2_z)V^{n-1}_{i,k} + D^\rho(V^{n-1}_{i,k}/\rho_i) + D^\rho(B^{n-1}_{i,k}/\rho_i)) \tag{181}$$

for $i,\ k = 2,3,\ldots N+1$. Then we impose the boundary conditions exactly as done in the first step. Finally we compute B^n_{ik} as explained above.

We notice that the second derivative in time is approximated by D_+D_- which is second-order accurate. The time step we use in all our runs is $\delta t = h/10$. The ratio $\delta t/h = 0.1$ satisfies the Courant condition, and we see from our runs that the whole method turns out to be numerically stable.

Besides the solution $V^n_{i,k}$ and $B^n_{i,k}$, an essential quantity we want to compute is the mass $m_\Omega(t)$, defined by (145) and (155), during the whole evolution. To this end we need to compute $\sigma(t)$ on the physical domain at all times. Given the approximations of $\bar{v}$ and β, we compute $\sigma(t)$ by integrating (149)—rewritten in terms of $\bar{v}$, as an ordinary differential equation (ODE) at each gridpoint. The initial data for these ODEs is computed by solving the elliptic Eq. (151), also rewritten in terms of $\bar{v}$, only once at initial time with homogeneous Dirichlet boundary conditions and using the same technique we use to compute β. The first time step to integrate (149) is carried out with explicit Euler method, and from there on with the two-step, second-order accurate, Leap-Frog method. We evaluate the integral in (155) with the midpoint rule.

VII. TESTS, RUNS AND NUMERICAL RESULTS

The numerical calculations we carry out in this work pursue two main objectives. The first objective is to make plausible that the initial-boundary value problem for (163) and (164) is well-posed. If we were simulating an IBVP that is not well-posed, the expectation would be that almost any consistent numerical simulation of the problem would fail to pass convergence tests, numerical stability tests, or both. We show below that both kinds of numerical tests are passed satisfactorily by our numerical approximation. The second objective is to study the behavior of the mass in these initial-boundary value problems. In particular, we will show that for fixed initial data, the larger the domain used in our calculation is, the longer and better the mass approaches a constant value.

We use in our runs two kinds of initial data which are smooth and strongly decaying outside a small region (Gaussian functions). The first is

$$\begin{aligned} \bar{v}_0(\rho, z) &= \exp\left(\frac{(\rho - 1/2)^2 + (z - L/2)^2}{0.1^2}\right), \\ \bar{v}_{0t}(\rho, z) &= 0, \end{aligned} \tag{182}$$

which decays very fast as (ρ, z) get away from $(1/2, L/2)$ and so approximate very well a compact support data on the domains we use. The second is the same kind of function but for $\bar{v}_{0t}$ instead of $\bar{v}_0$, namely

$$\begin{aligned} \bar{v}_0(\rho, z) &= 0, \\ \bar{v}_{0t}(\rho, z) &= 50\exp\left(\frac{(\rho - 1/2)^2 + (z - L/2)^2}{0.1^2}\right). \end{aligned} \tag{183}$$

Linearity of the problem tells us that the runs with $\bar{v}_0 \neq 0$, or $\bar{v}_{0t} \neq 0$ can be performed separately. A solution with general initial data is the superposition of two solutions, one with each kind of data.

b. Elliptic Solver Tolerance. We need to determine the value of ε to use in our runs. To this end we perform runs for six different values of ε with all other parameters fixed

to typical values in our runs. In these tests runs we use initial data given by (182) and Sommerfeld boundary conditions (166) and (168). We then analyze the different values of the mass obtained for the six solutions. By comparing the variations of $m_\Omega(t)$ with respect to the initial value of m_Ω, we see that our runs show that the evolution is not very sensitive to the tolerance ε. Figure 2 shows that the plot for the different computed masses superimpose when plotted in the full mass scale. The detail in the figure shows convergence of m_Ω as $\varepsilon \to 0$.

In Table I we show the maximum absolute difference between the computed masses with respect to the most accurate one (corresponding to $\varepsilon = 10^{-6}$) and the time of occurrence.

Based on this test we choose to use $\varepsilon = 10^{-3}$ in our further runs, which gives more the necessary accuracy for our discussion (around 10^{-6} relative error).

c. Convergence Tests. To study convergence of the numerical solution we perform two series of runs in a unitary square domain with the initial data (182). In the first series we use homogeneous Dirichlet boundary conditions and in the second Sommerfeld boundary conditions.

Each series consists of four runs. In the successive runs we use $h = 1/N$ with $N = 50; 100; 200; 400$. In all runs $\delta t = h/10$. Thus, in the second, third, and fourth runs both h and δt are divided by 2 with respect to the previous run. Let us call $V^{(h)}(t)$ the solution computed using mesh-size h.

TABLE I. Values of $\Delta m_\Omega = \max_t |m_{\Omega\varepsilon}(t) - m_{\Omega 10^{-6}}(t)|$ and time of occurrence for different values of the tolerance ε. Initial mass is $m_{\Omega 0} = 10.7083$.

ε	Δm_Ω	$t_{\max}$	$\delta m_\Omega / m_{\Omega 0}$
10^{-1}	1.27×10^{-3}	0.390	1.19×10^{-4}
10^{-2}	1.81×10^{-4}	0.406	1.69×10^{-5}
10^{-3}	1.45×10^{-5}	0.481	1.36×10^{-6}
10^{-4}	1.08×10^{-6}	0.503	1.01×10^{-7}
10^{-5}	8.19×10^{-8}	0.509	7.65×10^{-9}

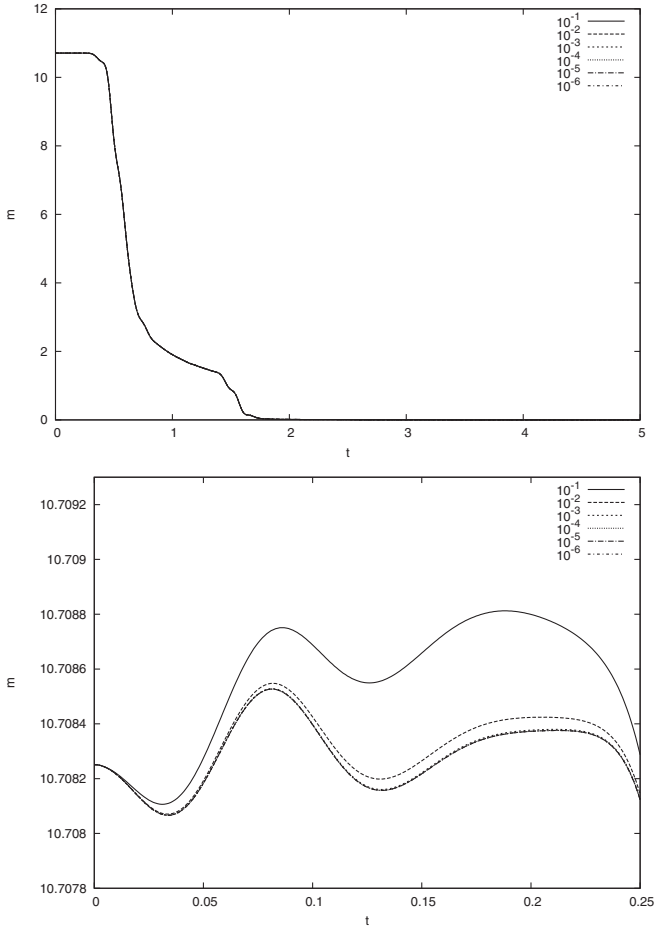

FIG. 2. Evolution of the mass for six different values of the tolerance ε. The upper plot shows the six runs in full mass scale. In this scale the six curves look superimposed. The lower plot shows a detail of the initial "flat" region in amplified scale.

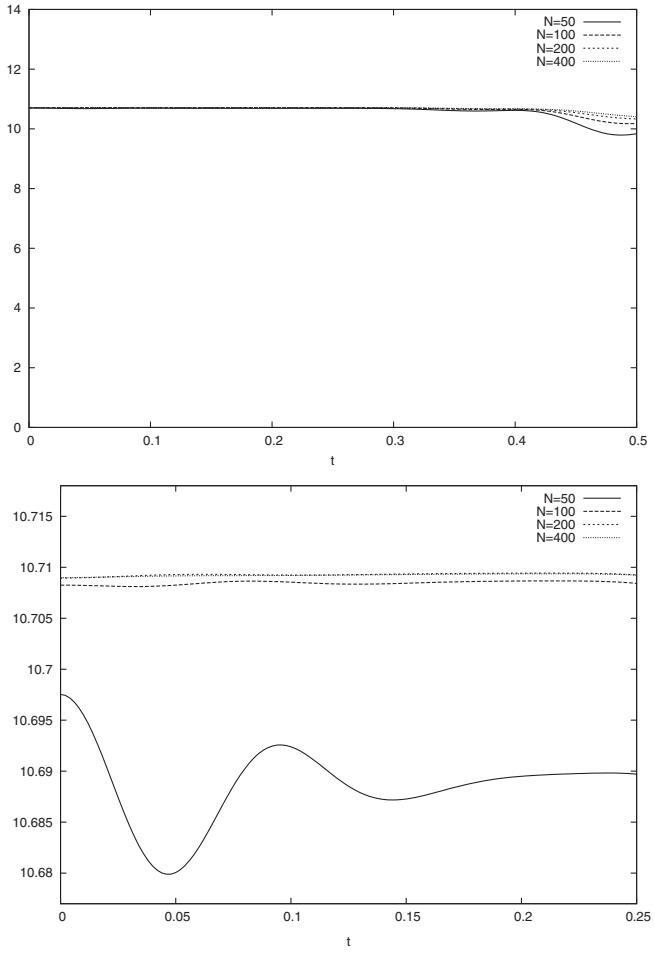

FIG. 3. Mass as function of time for evolution with homogeneous Dirichlet boundary conditions. In the upper plot, in full mass scale, the four curves look almost superimposed. In the lower plot a detail in expanded mass scale shows that the curves converge to a limit curve when h and δt diminish.

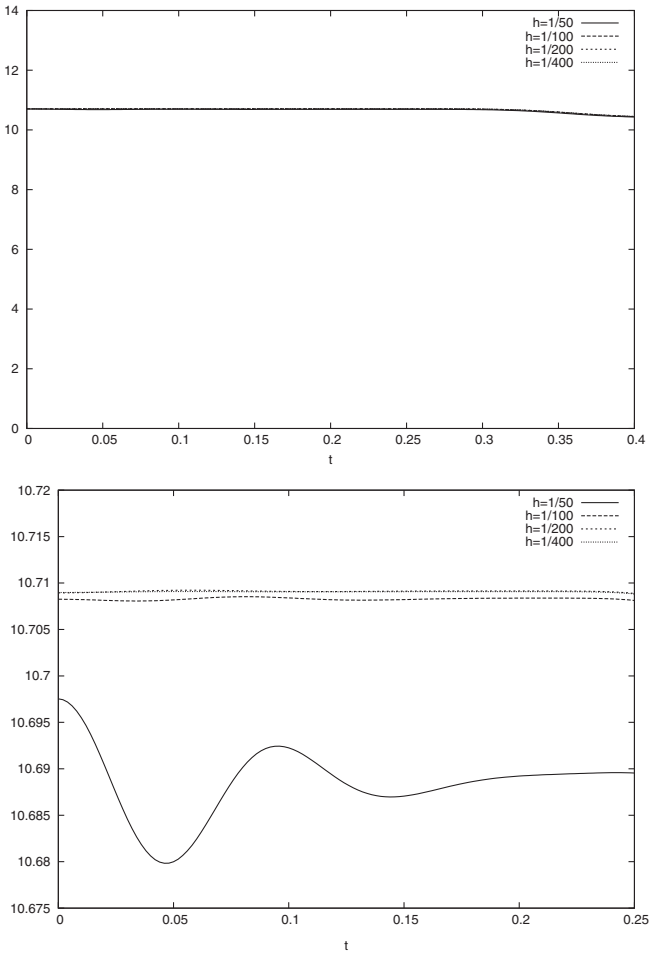

FIG. 4. Mass as function of time for evolution with Sommerfeld boundary conditions. In the upper plot, in full mass scale, the four curves look almost superimposed. In the lower plot a detail in expanded mass scale shows that the curves converge to a limit curve when h and δt diminish.

The first, simplest and indirect, convergence test is to plot the masses for each run as a function of time and check, graphically, whether they converge as the value of h diminishes. Figures 3 and 4 show that this is in fact the case.

A second more strict convergence and accuracy test is as follows. We compute the L_2 norm of the difference between two successive runs. A simple analysis shows that, when the method is convergent and the mesh and time-step sizes are small enough, the quotient

$$Q_h(t_n) = \frac{\|V^{(h)}(t_n) - V^{(h/2)}(t_n)\|_{L_2}}{\|V^{(h/2)}(t_n) - V^{(h/4)}(t_n)\|_{L_2}}, \tag{184}$$

approaches the value 2^p where p is the accuracy order of the method. Our method is fourth-order accurate in space and second-order in time. Therefore the expectation is that we obtain values of Q_h that are close to 4 at most times.

TABLE II. Convergence and accuracy quotient for solutions with homogeneous Dirichlet boundary condition. On the coarsest grid $h = 10^{-2}$.

t	$\|V^{(2)} - V^{(3)}\|_{L_2}$	$\|V^{(3)} - V^{(4)}\|_{L_2}$	$Q_h(t)$
0.05	5.2744×10^{-5}	1.3214×10^{-5}	3.9913
0.10	8.2053×10^{-5}	2.0665×10^{-5}	3.9706
0.15	9.2690×10^{-5}	2.3339×10^{-5}	3.9715
0.20	9.8158×10^{-5}	2.4938×10^{-5}	3.9360
0.25	1.1260×10^{-4}	2.8857×10^{-5}	3.9020
0.30	1.3325×10^{-4}	3.4668×10^{-5}	3.8436
0.35	1.6185×10^{-4}	4.4464×10^{-5}	3.6401
0.40	1.8421×10^{-4}	4.9874×10^{-5}	3.6934
0.45	2.2492×10^{-4}	6.9417×10^{-5}	3.2402
0.50	2.9719×10^{-4}	6.9240×10^{-5}	4.2923

To compute the L_2-norms we use the midpoint rule to approximate the integration on the coarsest grid of the two solutions being subtracted. Notice that the coarse grid is not a subgrid of the fine one, as they are displaced from the domain boundaries by different amounts. Then, to evaluate the finest solution on the coarse grid we need to interpolate this solution. To do this we use bilinear interpolation.

The results of this analysis are shown in Tables II and III. The test is passed satisfactorily.

d. Stability Tests. Numerical stability means that the solution to the IBVP stays bounded during time evolution. Typical signs of instability are the appearance of artifacts in the plot of the solution as a consequence of evolution and in most cases, after a while, the complete breakdown of the solution. If an instability has its root on the ill-posedness of the analytic problem underneath, the expectation is that some high frequency modes of the solution explode exponentially fast and are detected at very short times of the numerical evolution. For some more benign ill-posed problems (like weakly hyperbolic problems) the growing of instabilities is only polynomial and it may take longer to detect them.

TABLE III. Convergence and accuracy quotient for solutions with Sommerfeld boundary condition. On the coarsest grid $h = 10^{-2}$.

t	$\|V^{(2)} - V^{(3)}\|_{L_2}$	$\|V^{(3)} - V^{(4)}\|_{L_2}$	$Q_h(t)$
0.04	6.6922×10^{-5}	1.6703×10^{-5}	4.0067
0.08	6.2007×10^{-5}	1.5756×10^{-5}	3.9355
0.12	9.1495×10^{-5}	2.2958×10^{-5}	3.9854
0.16	9.2694×10^{-5}	2.3357×10^{-5}	3.9686
0.20	9.8226×10^{-5}	2.4911×10^{-5}	3.9431
0.24	1.0935×10^{-4}	2.7940×10^{-5}	3.9138
0.28	1.2407×10^{-4}	3.2083×10^{-5}	3.8671
0.32	1.4427×10^{-4}	3.8153×10^{-5}	3.7813
0.36	1.6740×10^{-4}	4.6440×10^{-5}	3.6047
0.40	1.8389×10^{-4}	5.0471×10^{-5}	3.6434

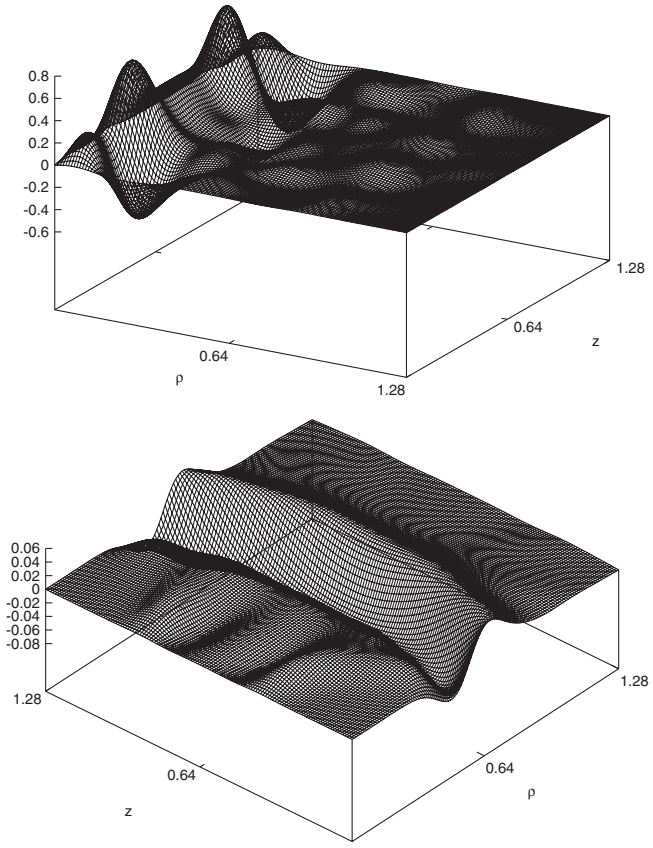

FIG. 5. Plots of the solution $\bar{v}(t)$. Both plots of solutions computed on a grid with 128×128 gridpoints and initial data given by (182). Upper plot is the solution with homogeneous Dirichlet boundary conditions at time $t = 3.0$, while lower plot is the solution with Sommerfeld boundary conditions at time $t = 1.25$.

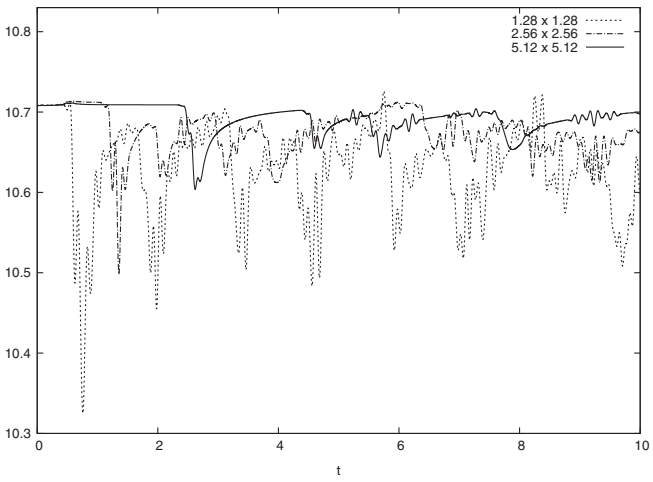

FIG. 6. Evolution of the mass m_Ω as a function of time for three solutions with homogeneous Dirichlet boundary conditions and the same initial data but on domains of different size. In the upper right corner each curve is associated to the corresponding domain.

We performed several series of runs using both kinds of boundary conditions (166) and (167) or (166) and (168) and both kinds of initial data (182) or (183) on different domains and during several time intervals. We studied the plots of the solutions in all cases and they always look smooth, agreement with the boundary conditions imposed, and never showed any sort of strange artifact. Typical plots for $\bar{v}(\rho, z, t)$ are shown in Fig. 5. We have also studied the plots of $\beta(\rho, z, t)$ in these runs and no sign of instability showed.

A second, physically meaningful, test for stability is provided by the study of the mass m_Ω which in this problem is a sort of incomplete H^2 Sobolev norm of the solution. As explained in Sec. V the mass is conserved for the Cauchy problem in the whole space. On bounded domains this is no longer true, but we expect that it stays bounded when using homogeneous Dirichlet boundary conditions, and that it goes to zero when using

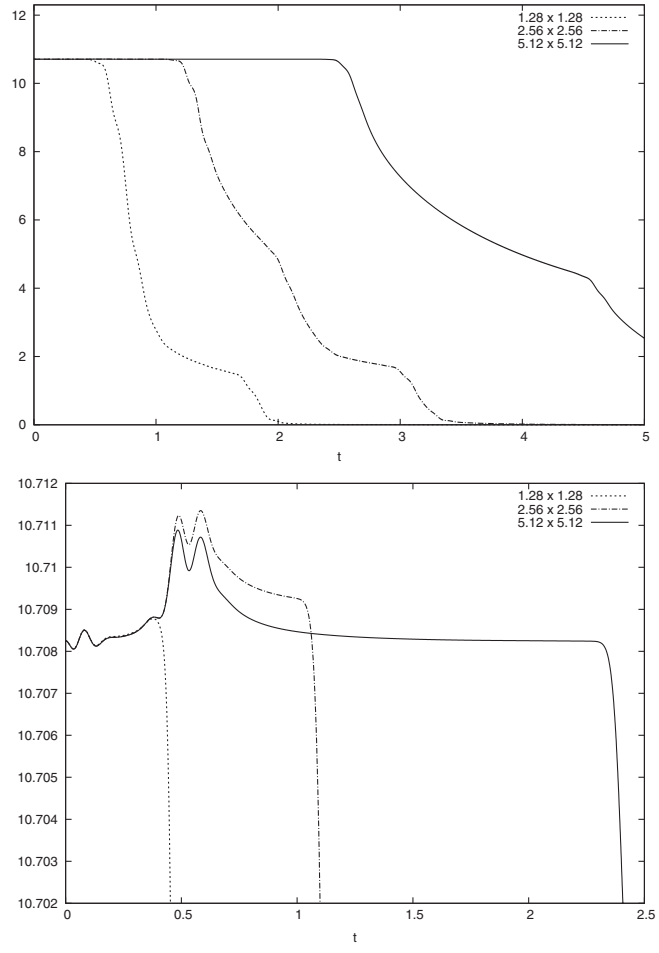

FIG. 7. Evolution of the mass m_Ω as a function of time for three solutions with Sommerfeld boundary conditions, the same initial data but on domains of different size. In the upper right corner each curve is associated to the corresponding domain. The lower plot shows in amplified scale that the flat region presents very small variations of around 0.03%.

Sommerfeld boundary conditions. We analyze the behavior of the mass below.

e. Behavior of the Mass. As explained before the mass, defined by (145) and (155), is a conserved quantity when the Cauchy problem is considered in the whole space (i.e., Ω is $\mathbb{R}^2_+$). In our numerical tests we solve the initial-boundary value problem on compact domains where no known boundary conditions imply mass conservation. However, an interesting study for the mass evolution can be done as follows. We solve the IBVP on domains of different size but use, in all runs, the same initial data, at the same distance from the symmetry axis. The initial data are chosen to decay exponentially fast outside a region which is small compared to the smallest of the domains we use. Clearly, the expectation is that the larger the domain is the closest to constant the mass stays during evolution.

We do a series of runs for homogeneous Dirichlet boundary conditions and for Sommerfeld (outgoing waves) boundary conditions. The plots for the Dirichlet case are shown in Fig. 6. Observe that the plot is not on full mass scale. The three curves show an almost constant initial region and then variations of small relative amplitude. After an initial peak immediately after the constant region the amplitude of the variations is, roughly speaking, 2% for the 1.28×1.28 domain, 1% for the 2.56×2.56 domain, and 0.6% for the 5.12×5.12 domain. The amplitude clearly diminishes when the domain increases size. For the case of Sommerfeld boundary conditions, the plots of the mass evolution can be seen in Fig. 7. This series of three runs is totally analogous to the previous case. The only change is the boundary condition used. As can be inferred from the plot in full mass scale, the energy leaks though the boundary as expected.

VIII. FINAL COMMENTS

In this article we have deduced the linear system (1) and (2) and we have analyzed some of its properties. Among them, the most relevant are the mass conservation and the numerical stability. The main open problem is to prove that this system is well-posed. Remarkably enough, there seems to be not much literature on this class of linear systems which are singular at the axis.

Once the well-posedness problem is solved, we believe that the future research on the subject can be divided in two parallel but complementary roads. The first one is to extend the well-posedness from the linear system to the full Einstein equations in the maximal-isothermal gauge. The nonlinear lower-order terms introduce extra difficulties (see [6]). There are many possible evolution schemes (see the discussion in [7]). It is very likely that few of them (or may be only one) are well-posed. If this is the case, the resolution of the well-posedness question will lead us to select (or even discover) the correct evolution scheme. After the local problem is solved, the next step is to use the global conservation of the mass to control the full nonlinear evolution in this gauge. A natural first example would be to recover the nonlinear stability of Minkowski [29] in this gauge. The expectation is that the mass formula will provide a simpler (and different) kind of approach to this problem; although, of course, always restricted to axial symmetry. The ultimate and difficult goal is to say something, in this gauge, about the nonlinear stability of a black hole in axial symmetry.

The second road is the study of axially symmetric perturbations but with a black hole as background solution. Linear stability of the Kerr black hole is a relevant open problem which is currently intensively studied (see the review articles [30,31] and references therein). The expectation is that the mass formula can help to prove linear stability under axially symmetric perturbations of the Kerr black hole.

ACKNOWLEDGMENTS

S. D. thanks Piotr Chruściel and Helmut Friedrich for useful discussions. These discussions took place at the Mathematisches Forschungsinstitut Oberwolfach during the workshop "Mathematical Aspects of General Relativity," October 11th–October 17th, 2009. S. D. thanks Andrés Aceña for useful discussions that took place at the Max-Planck-Institut für Gravitationsphysik (Albert-Einstein-Institut) during the conference "Space, Time and Beyond", October 19th–October 21th, 2009. S. D. thanks the organizers of these events for the invitation and the hospitality and support of the Mathematisches Forschungsinstitut Oberwolfach and the Max-Planck-Institut für Gravitationsphysik (Albert-Einstein-Institut). S. D. is supported by CONICET (Argentina). This work was supported in part by Grant No. PIP 6354/05 of CONICET (Argentina), Grant No. 05/B415 Secyt-UNC (Argentina) and the Partner Group grant of the Max Planck Institute for Gravitational Physics, Albert-Einstein-Institute (Germany).

APPENDIX: USEFUL FORMULAS

We collect in this appendix some useful formulas that are used in the main part of this article. The conformal Killing operator in two dimensions with respect to the metric q_{AB} is defined by

$$(\mathcal{L}_q \beta)_{AB} = D_A \beta_B + D_B \beta_A - q_{AB} D_C \beta^C. \tag{A1}$$

For the particular case of a flat metric δ_{AB} this definition reduces to

$$(\mathcal{L} \beta)_{AB} = \partial_A \beta_B + \partial_B \beta_A - \delta_{AB} \partial_C \beta^C. \tag{A2}$$

For this operator we have the following identity often used in the article:

$$\partial^B (\mathcal{L} \beta)_{AB} = \Delta \beta_A. \tag{A3}$$

The Christofell symbols of the metric q_{AB} defined by (57) are given by

$$\Gamma^C_{AB} = \delta^C_B \partial_A u + \delta^C_A \partial_B u - \partial^C u \delta_{AB}, \tag{A4}$$

and the Ricci tensor is given by

$$^{(2)}R_{AB} = -\Delta u \delta_{AB}, \qquad ^{(2)}R = -2e^{-2u}\Delta u. \tag{A5}$$

Under the conformal rescaling (56) the diferential operators relevant in this article transform as follows:

$$\Delta_q f = e^{-2u}\Delta f, \tag{A6}$$

$$\mathcal{L}_q(\beta)_{AB} = e^{2u}\mathcal{L}(\hat{\beta})_{AB}, \tag{A7}$$

$$D_B \chi^{AB} = e^{-4u}\partial_B \hat{\chi}^{AB}, \tag{A8}$$

where we have defined

$$\beta_A = e^{2u}\hat{\beta}_A \qquad \chi^{AB} = e^{-4u}\hat{\chi}^{AB}. \tag{A9}$$

We follow the convention that the indices for hat quantities are moved with the flat metric δ_{AB} and indices of nonhat quantities with the metric q_{AB}. Then, we have

$$\chi_{AB} = \hat{\chi}_{AB}, \qquad \beta^A = \hat{\beta}^A. \tag{A10}$$

That is why we suppress the hat notation for the tensors $\hat{\chi}_{AB}$ and $\hat{\beta}^A$ in the main part of this article.

Take an arbitrary spacelike foliation on $(\mathcal{N}, h_{ab})$. The $2+1$ decomposition of the wave operator is given by

$$\Box f = -f'' + \Delta_q f + D_A f \frac{D^A \alpha}{\alpha} + f' \chi, \tag{A11}$$

where have made use of the following useful formulas:

$$n^a \nabla_a n_A = \frac{\partial_A \alpha}{\alpha}, \qquad n^a \nabla_a n_t = \frac{\beta^A \partial_A \alpha}{\alpha}. \tag{A12}$$

[1] J. Bičák and A. Pravdová, J. Math. Phys. (N.Y.) **39**, 6011 (1998).
[2] R. Geroch, J. Math. Phys. (N.Y.) **12**, 918 (1971).
[3] M. Alcubierre, *Introduction to* 3 + 1 *Numerical Relativity*, International Series of Monographs on Physics (Oxford University Press, Oxford, United Kingdom, 2008).
[4] D. Garfinkle and G. C. Duncan, Phys. Rev. D **63**, 044011 (2001).
[5] M. W. Choptuik, E. W. Hirschmann, S. L. Liebling, and F. Pretorius, Classical Quantum Gravity **20**, 1857 (2003).
[6] O. Rinne, Classical Quantum Gravity **25**, 135009 (2008).
[7] O. Rinne, Ph.D. thesis, University of Cambridge, 2005.
[8] M. Ruiz, M. Alcubierre, and D. Nunez, Gen. Relativ. Gravit. **40**, 159 (2008).
[9] A. D. Rendall, Living Rev. Relativity **8** (2005), 6.
[10] S. Dain, Classical Quantum Gravity **25**, 145021 (2008).
[11] S. Dain, Int. J. Mod. Phys. D **17**, 519 (2008).
[12] J. M. Bardeen and T. Piran, Phys. Rep. **96**, 205 (1983).
[13] T. Nakamura, K. Oohara, and Y. Kojima, Prog. Theor. Phys. Suppl. **90**, 1 (1987).
[14] O. Rinne and J. M. Stewart, Classical Quantum Gravity **22**, 1143 (2005).
[15] E. Sorkin, arXiv:0911.2011.
[16] G. Weinstein, Commun. Pure Appl. Math. **43**, 903 (1990).
[17] Y. Choquet-Bruhat and V. Moncrief, Ann. Inst. Henri Poincaré **2**, 1007 (2001).
[18] Y. Choquet-Bruhat, in *The Einstein Equations and The Large Scale Behavior of Gravitational Fields*, edited by P. T. Chruściel and H. Friedrich (Birkhäuser, Basel, 2004), pp. 251–298.
[19] L. Andersson, in *The Einstein Equations and The Large Scale Behavior of Gravitational Fields*, edited by P. T. Chruściel and H. Friedrich (Birkhäuser, Basel, 2004), pp. 71–120.
[20] A. Rendall, *Partial Differential Equations in General Relativity (Oxford Graduate Texts in Mathematics)* (Oxford University Press, Oxford, United Kingdom, 2008).
[21] A. Rendall, 3 + 1 (2008), URL http://www.aei.mpg.de/rendall/3+1.ps.
[22] Y. Choquet-Bruhat and J. W. York, Jr., arXiv:gr-qc/9601030.
[23] H.-O. Kreiss and J. Lorenz, *Initial-boundary Value Problems and the Navier-Stokes Equations*, Pure and Applied Mathematics Vol. 136 (Academic Press Inc., Boston, MA, 1989).
[24] S. Dain (unpublished).
[25] H.-O. Kreiss and O. E. Ortiz, in *The Conformal Structure of Spacetimes: Geometry, Analysis, Numerics*, Lecture Notes in Physics Vol. 604, edited by J. Frauendiener and H. Friedrich (Springer, New York, 2002), pp. 359–370.
[26] H. O. Kreiss and J. Winicour, Classical Quantum Gravity **23**, S405 (2006).
[27] H. O. Kreiss, O. Reula, O. Sarbach, and J. Winicour, Classical Quantum Gravity **24**, 5973 (2007).
[28] B. Gustafsson, H.-O. Kreiss, and J. Oliger, *Pure and Applied Mathematics* (John Wiley & Sons Inc., New York, 1995).
[29] D. Christodoulou and S. Klainerman, *The Global Nonlinear Stability of the Minkowski Space*, Princeton Mathematical Series Vol. 41 (Princeton University Press, Princeton, NJ, 1993).
[30] F. Finster, N. Kamran, J. Smoller, and S.-T. Yau, arXiv:0801.1423.
[31] M. Dafermos and I. Rodnianski, arXiv:0811.0354.